

Reconstruction of a direction-dependent primordial power spectrum from Planck CMB data

Amel Durakovic,^a Paul Hunt,^b Suvodip Mukherjee,^{c,d,e,f} Subir Sarkar,^{a,b} Tarun Souradeep^f

^aNiels Bohr Institute, Blegdamsvej 17, DK-2100 Copenhagen, Denmark

^bRudolf Peierls Centre for Theoretical Physics, 1 Keble Road, Oxford OX1 3NP, UK

^cCenter for Computational Astrophysics, Flatiron Institute, 162 5th Avenue, New York, NY 10010, USA

^dInstitut d'astrophysique de Paris, 98 bis Bld Arago, 75014 Paris, France

^eInstitut Lagrange de Paris, Sorbonne Universités, 98 bis Bld Arago, 75014 Paris, France

^fInter-University Centre for Astronomy and Astrophysics, Post Bag 4, Ganeshkind, Pune 411007, India

E-mail: amel@nbi.dk, smukherjee@flatironinstitute.org, s.sarkar@physics.ox.ac.uk, tarun@iucaa.in

Abstract. We consider the possibility that the primordial curvature perturbation is direction-dependent. To first order this is parameterised by a quadrupolar modulation of the power spectrum and results in statistical anisotropy of the cosmic microwave background, which can be quantified using the bipolar spherical harmonic representation. We compute these for the Planck Release 2 SMICA map and use them to infer the quadrupole modulation of the primordial power spectrum which, going beyond previous work, we allow to be *scale-dependent*. Uncertainties are estimated from Planck FFP9 simulations. Consistent with the Planck collaboration's findings, we find no evidence for a constant quadrupole modulation, nor one scaling with wave number as a power law. However our non-parametric reconstruction suggests several spectral features. When a constant quadrupole modulation is fitted to data limited to the wave number range $0.005 \leq k/\text{Mpc}^{-1} \leq 0.008$, we find that its preferred direction is *aligned* with the cosmic hemispherical asymmetry. To determine the statistical significance we construct two different test statistics and test them on our reconstructions from data, against reconstructions of realisations of noise only. With a test statistic sensitive only to the amplitude of the modulation, the reconstructions are unusual at 2.5σ significance in the full wave number range, but at 2.2σ when limited to the intermediate wave number range $0.008 \leq k/\text{Mpc}^{-1} \leq 0.074$. With the second test statistic, sensitive also to direction, the reconstructions are unusual with 4.6σ significance, dropping to 2.7σ for the intermediate wave number range. Our approach is easily generalised to include other data sets such as polarisation, large-scale structure and forthcoming 21-cm line observations which will enable these anomalies to be investigated further.

Keywords: Statistical anisotropy, primordial power spectrum, reconstruction, quadrupole modulation, BipoSH, CMB, Tikhonov regularisation

Contents

1	Introduction	1
2	Formalism	3
3	Setup and tests	7
4	Results	11
4.1	Scale-independent quadrupole modulation	11
4.2	Power-law quadrupole modulations	13
4.3	Non-parametric quadrupole modulations	14
5	Statistical significance of a quadrupole modulation	16
5.1	Power law quadrupole modulations	16
5.2	Non-parametric quadrupole modulations	18
6	Summary and conclusion	20
A	Relating quadrupole modulations to BipoSH coefficients	23
B	Other choices of λ	25
C	The distribution of T	25
D	The Anderson-Darling test	29

1 Introduction

The anisotropies of the cosmic microwave background (CMB) are believed to have been seeded by curvature perturbations generated at an earlier stage in the evolution of the universe. The most discussed mechanism for this is the quantum fluctuations of a scalar field, the vacuum energy of which drives a period of accelerated expansion known as inflation. In the simplest scenario where the ‘inflaton’ field evolves slowly down an almost flat potential, the (dimensionless) primordial power spectrum, which is the variance of the Fourier components of the curvature perturbation, is predicted to be almost scale invariant, with slightly more power on large scales. Provided that the primordial power spectrum is independent of the direction (and the background cosmology is homogeneous and isotropic), the anisotropies of the CMB will also be statistically isotropic.

We consider here the possibility of a direction-*dependent* primordial power spectrum resulting in statistically anisotropic fluctuations of the CMB. In order for this to occur, some field must single out a particular direction u^μ and break rotational symmetry, and so the agent should either carry a space-time index or have a spatial gradient present in the initial field configuration. The first such model [1] considered a vector field A^μ driving inflation via the effective scalar $\xi = A_\mu A^\mu$ with a sufficiently flat potential $V(\xi)$. When the vector field singles out a direction, its energy-momentum tensor is no longer isotropic, so its direction-dependence can play a role gravitationally; in this case, inflation is followed by

anisotropic expansion. Other work, motivated by some observational CMB anomalies, found that an anisotropy in the initial expansion rate following inflation can cause the fluctuations to inherit the anisotropy [2]. A concrete realisation of the anisotropy, with a vector field responsible, was subsequently proposed [3]. Such vector field models were, however, found to be unstable [4, 5]. Another possibility is that the vector field couples to the inflaton and thereby transfers the anisotropy, as in models with a coupling $f(\phi)^2 F_{\mu\nu} F^{\mu\nu}$ where $f(\phi)$ is a function of the inflaton field and $F_{\mu\nu} = \partial_\mu A_\nu - \partial_\nu A_\mu$ is the field strength of the vector field A_μ [6]. It is important that the anisotropic field should *not* contribute significantly to the energy density, otherwise the expansion itself will be anisotropic to a degree in conflict with observations. This can be circumvented however by invoking an additional light scalar field that generates the perturbations but has an initial spatial gradient that is responsible for the statistical anisotropy [7].

Such models can produce an angular modulation [8] such that the full (dimensionless) primordial power spectrum is:

$$\mathcal{P}(\mathbf{k}) = \mathcal{P}(k) + \sqrt{4\pi} \sum_{M=-L}^L g_{LM}(k) Y_{LM}(\hat{\mathbf{k}}). \quad (1.1)$$

We focus on the quadrupole modulation ($L = 2$)

$$\mathcal{P}(\mathbf{k}) = \mathcal{P}(k) + \sqrt{4\pi} \sum_{M=-2}^2 g_{2M}(k) Y_{2M}(\hat{\mathbf{k}}), \quad (1.2)$$

where $\mathcal{P}(k)$ is the usual isotropic power spectrum, $Y_{2M}(\hat{\mathbf{k}})$ are spherical harmonics that carry the direction-dependence and $g_{2M}(k)$ are the associated coefficients which may vary with the wave number k and be either positive or negative. As the coefficients $g_{2M}(k)$ determine the modulation, they are our main focus for reconstruction from data. Note that we have specifically chosen the split (1.2) in order to remain agnostic about the isotropic part of the primordial power spectrum, unlike the alternative parameterisation

$$\mathcal{P}(\mathbf{k}) = \mathcal{P}(k)(1 + g(k)(\hat{\mathbf{k}} \cdot \hat{\mathbf{n}})^2), \quad (1.3)$$

which reconstructs the shape of the quadrupole modulation relative to the isotropic primordial power spectrum. By contrast we reconstruct the *absolute* quadrupole modulation.

Symmetry considerations dictate that the quadrupole is the first modulation that can appear. The next contribution would be the hexadecapole $L = 4$ as only even L are allowed (see § 2). Since the $L = 2$ modulation is the first one that can appear and also has some theoretical motivation we will consider only this case although our formalism readily allows for the inclusion of higher order modulations.

The quadrupole modulation of the primordial power spectrum will manifest itself in the CMB temperature fluctuations which will now be statistically anisotropic. The temperature fluctuations ΔT are conventionally expanded in spherical harmonics such that

$$\Delta T(\theta, \phi) = \sum_{\ell m} a_{\ell m} Y_{\ell m}(\theta, \phi). \quad (1.4)$$

For statistical isotropy, the correlation function is:

$$\langle a_{\ell m} a_{\ell' m'}^* \rangle = C_\ell \delta_{\ell\ell'} \delta_{mm'}, \quad (1.5)$$

where C_ℓ is the (isotropic) angular power spectrum and the brackets indicate ensemble averages. In the statistically *anisotropic* case, this no longer holds and there are additional terms with ‘bipolar spherical harmonics’ (BipoSH) coefficients. The BipoSH coefficients associated with a given multipole modulation can readily be calculated and in turn given the BipoSH coefficients of a CMB map, it is possible to reconstruct the direction-dependent primordial power spectrum. Previous work by the Planck collaboration to extract this from their CMB maps has assumed a constant value of the quadrupole modulation [9] or a smooth power-law scale dependence [10]. However, in addition to these exercises, we will reconstruct the full spectrum from Planck data, allowing for the quadrupole modulation to vary *freely* with wave number. We follow an approach to reconstruction based on ‘Tikhonov regularisation’ that has been demonstrated to work well for isotropic primordial power spectra [11, 12].

This paper is organised as follows. In Section 2, the detailed formalism is presented: BipoSH coefficients are defined and related to quadrupole modulations and Tikhonov regularisation is described. In Section 3, estimates of uncertainties are made using the latest Planck Full Focal Plane (FFP9) simulations [13] and used to construct a simplified likelihood for binned data which is then tested. The reconstruction is performed on benchmark spectra adopting the estimated uncertainties, in order to check how well it performs. In Section 4, the data is presented. Results of best-fit constant and power-law quadrupole modulations to this data set are then presented followed by our main results, the non-parametric reconstructions. In Section 5, the statistical significance of possible spectral features is discussed. We summarise in Section 6.

2 Formalism

The general two-point function of spherical harmonics coefficients can be written

$$\langle a_{\ell m} a_{\ell' m'}^* \rangle = C_\ell \delta_{\ell\ell'} \delta_{mm'} + \sum_{LM} (-1)^{m'} C_{\ell m \ell' -m'}^{LM} A_{\ell\ell'}^{LM}, \quad (2.1)$$

where $C_{\ell m \ell' -m'}^{LM}$ are Clebsch-Gordan coefficients and $A_{\ell\ell'}^{LM}$ are BipoSH coefficients [14, 15]. These are associated with the *bipolar* spherical harmonics which form an orthonormal basis for functions of two directions. This is most evident when considering the temperature correlation function in real space

$$\begin{aligned} C(\hat{\mathbf{n}}, \hat{\mathbf{n}}') &= \langle \Delta T(\hat{\mathbf{n}}) \Delta T(\hat{\mathbf{n}}') \rangle = \sum_{\ell\ell' LM} A_{\ell\ell'}^{LM} \{Y_\ell(\hat{\mathbf{n}}) \otimes Y_{\ell'}(\hat{\mathbf{n}}')\}_{LM} \\ &= \sum_{\ell} \frac{2\ell+1}{4\pi} C_\ell P_\ell(\hat{\mathbf{n}} \cdot \hat{\mathbf{n}}') + \sum_{\ell\ell' LM} A_{\ell\ell'}^{LM} \{Y_\ell(\hat{\mathbf{n}}) \otimes Y_{\ell'}(\hat{\mathbf{n}}')\}_{LM}, \end{aligned} \quad (2.2)$$

where,

$$\{Y_\ell(\hat{\mathbf{n}}) \otimes Y_{\ell'}(\hat{\mathbf{n}}')\}_{LM} = \sum_{mm'} C_{\ell m \ell' -m'}^{LM} Y_{\ell m}(\hat{\mathbf{n}}) Y_{\ell' m'}(\hat{\mathbf{n}}'). \quad (2.3)$$

Just as the spherical harmonics coefficients can be calculated from a map by projection onto the basis functions, $a_{\ell m} = \int d\Omega Y_{\ell m}^*(\hat{\mathbf{n}}) T(\hat{\mathbf{n}})$, the BipoSH coefficients can be similarly computed as

$$A_{\ell\ell'}^{LM} = \int d\Omega \int d\Omega' C(\hat{\mathbf{n}}, \hat{\mathbf{n}}') \{Y_\ell(\hat{\mathbf{n}}) \otimes Y_{\ell'}(\hat{\mathbf{n}}')\}_{LM}^*. \quad (2.4)$$

This can be written more straightforwardly in terms of the spherical harmonics as

$$A_{\ell\ell'}^{LM} = \sum_{m m'} \langle a_{\ell m} a_{\ell' m'} \rangle (-1)^{m'} C_{\ell m \ell' -m'}^{LM}, \quad (2.5)$$

which can have both even and odd parity [16]. Only the *even* parity BipoSH coefficients are non-zero for a quadrupolar modulation of the power spectrum and these are related to the even parity BipoSH spectra as:

$$A_{\ell\ell'}^{LM} = \sqrt{\frac{(2\ell+1)(2\ell'+1)}{2L+1}} C_{\ell 0 \ell' 0}^{L,0} A_{\ell\ell'}^{LM}. \quad (2.6)$$

We adopt this definition in our work, following the WMAP collaboration [17].

The dimensionful primordial power spectrum $P(\mathbf{k})$ is the variance of the curvature perturbation $\mathcal{R}(\mathbf{k})$ such that

$$\langle \mathcal{R}(\mathbf{k}) \mathcal{R}(\mathbf{k}') \rangle = (2\pi)^3 \delta^{(3)}(\mathbf{k} + \mathbf{k}') P(\mathbf{k}), \quad (2.7)$$

which under a reflection of the vectors on both sides implies that $P(-\mathbf{k}) = P(\mathbf{k})$. Since the spherical harmonics are inside $P(\mathbf{k})$, only those spherical harmonics which equal themselves upon reflection are admitted, and this holds for the even L only. It is useful to note that since $Y_{LM}^*(\hat{\mathbf{k}}) = (-1)^M Y_{LM}(\hat{\mathbf{k}})$, in order for $P(\mathbf{k})$ to be real-valued, it must be the case that $g_{LM}^*(k) = (-1)^M g_{LM}(k)$. This means that it is only necessary to reconstruct g_{LM} for non-negative M .

The central relation is that between the direction-dependent modulations of the primordial power spectrum and the induced BipoSH coefficients associated with the temperature anisotropies. The coefficients are:

$$A_{\ell\ell'}^{LM} = 4\pi (-i)^{\ell-\ell'} \int_0^\infty d \log k g_{LM}(k) \Delta_\ell(k) \Delta_{\ell'}(k), \quad (2.8)$$

where $\Delta_\ell(k)$ are temperature transfer functions relating curvature perturbations $\mathcal{R}(k)$ to multipoles of the temperature perturbations. This relation is derived in Appendix A.

It is useful to introduce another variable d that counts the distance from ℓ to $\ell' \equiv \ell + d$. It will only be necessary to compute for $d = 0$ and $d = 2$ since the BipoSH coefficient $A_{\ell\ell'}^{LM}$ appears with the Clebsch-Gordan coefficient $C_{\ell m \ell' -m'}^{LM}$ which for $L = 2$ is non-zero only when ℓ and ℓ' are equal or differ by two. It will not be necessary to calculate for $d = -2$ as eq.(2.8) is symmetric in ℓ and ℓ' so that $A_{\ell \ell-2}^{2M}$ is equal to $A_{\ell-2 \ell}^{2M}$. Similarly the hexadecapole would require the calculation for $d = 0, 2, 4$.

In order to make the problem of reconstruction amenable to numerical analysis, an evenly spaced grid in $\log k$ space at positions k_i is introduced and made sufficiently fine that its discretisation does not matter. The modulation $g_{LM}(k)$ is then written in terms of functions $\phi_j(k)$ that are equal to unity in the space between the grid points k_j and k_{j+1} and zero otherwise, such that

$$g_{LM}(k) = \sum_i g_i^{LM} \phi_i(k), \quad (2.9)$$

where g_i^{LM} are now coefficients. Upon introducing q as a collective variable for ℓ and d , eq.(2.8) can now be written as a matrix equation

$$A_q^{LM} = \sum_i W_{qj} g_j^{LM} \Leftrightarrow \mathbf{A}^{LM} = \mathbf{W} \mathbf{g}^{LM}, \quad (2.10)$$

where \mathbf{A}^{LM} and \mathbf{g}^{LM} are vectors and the matrix \mathbf{W} is given by

$$W_{qj} = 4\pi i^d \int_0^\infty d \log k \phi_j(k) \Delta_\ell(k) \Delta_{\ell+d}(k). \quad (2.11)$$

Since W_{qj} is always real, it is convenient to split \mathbf{g}^{LM} into a real and an imaginary part that contribute to $\text{Re } \mathbf{A}^{LM}$ and $\text{Im } \mathbf{A}^{LM}$, respectively. Let the complex-valued vector \mathbf{g}^{LM} be redefined such that the imaginary part of \mathbf{g}^{LM} be put after the real part of \mathbf{g}^{LM} in a real-valued vector

$$\mathbf{g}^{LM} := \begin{pmatrix} \text{Re } \mathbf{g}^{LM} \\ \text{Im } \mathbf{g}^{LM} \end{pmatrix}. \text{ Similarly, } \mathbf{A}^{LM} := \begin{pmatrix} \text{Re } \mathbf{A}^{LM} \\ \text{Im } \mathbf{A}^{LM} \end{pmatrix} \text{ and } \mathbf{W} := \begin{pmatrix} \mathbf{W} & \\ & \mathbf{W} \end{pmatrix} \quad (2.12)$$

becomes a block matrix. The matrix \mathbf{W} , which relates a given modulation \mathbf{g}^{LM} to the BipoSH coefficients \mathbf{A}^{LM} , has a non-trivial kernel, so the matrix equation (2.10) *cannot* be inverted to obtain the required \mathbf{g}^{LM} . Physically, this is due to projection effects wherein one mode contributes to many BipoSH coefficients so it is impossible to invert the relation without additional assumptions. This is illustrated in Fig. 1 where different rows of \mathbf{W} are plotted, relating the contribution of a mode k to the BipoSH coefficient associated with one of the curves.

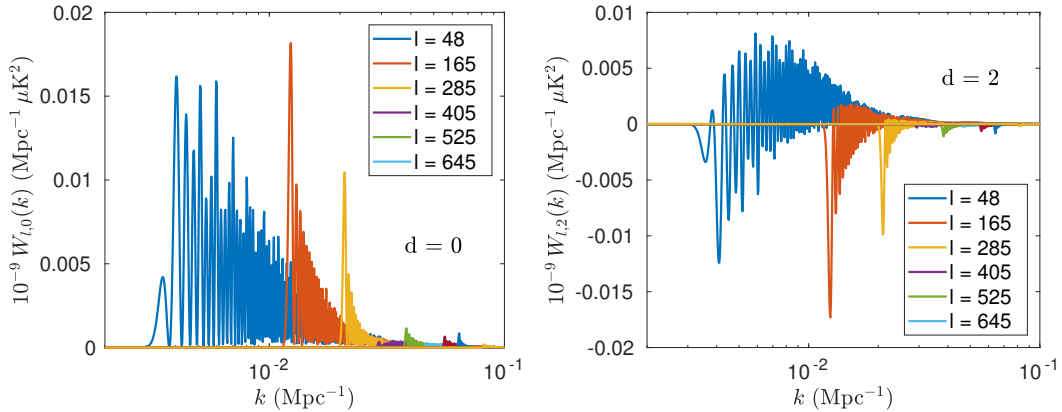


Figure 1. The transfer functions W_{qk} relating g_k^{LM} to $A_{\ell d}^{LM}$ for $d = 0$ (left panel) and $d = 2$ (right panel) and representative choices of the multipole ℓ . As a rule of thumb, the maxima are near $k = \ell \eta_0^{-1} \approx \ell / 14,000 \text{ Mpc}^{-1}$, where η_0 is the conformal time today.

In order to proceed further, this deconvolution problem needs regularisation. We opt to choose that solution $\hat{\mathbf{g}}^{LM}$ amongst the multitude of otherwise equally likely solutions which has the least ‘roughness’ $R(\mathbf{g}^{LM})$. This is defined, in the continuous case, as

$$R(g_{LM}) = \int dk \left(\frac{d \text{Re } g_{LM}(k)}{d \log k} \right)^2 + \int dk \left(\frac{d \text{Im } g_{LM}(k)}{d \log k} \right)^2, \quad (2.13)$$

while, in the discrete case, it is

$$R(\mathbf{g}^{LM}) = (\mathbf{g}^{LM})^T \mathbf{\Gamma} \mathbf{g}^{LM}, \quad (2.14)$$

and $\mathbf{H}^{LM} = \mathbf{W}^T \boldsymbol{\Sigma}^{LM-1} \mathbf{W} + \lambda \boldsymbol{\Gamma}$ is the Hessian.

It is also useful to consider the frequentist covariance matrix. It is simply the error in $\hat{\mathbf{g}}^{LM}$ that is induced by the error in the data $\tilde{\mathbf{A}}^{LM}$. Since $\hat{\mathbf{g}}^{LM}$ and $\tilde{\mathbf{A}}^{LM}$ are related by a linear transformation (2.19), the (frequentist) covariance matrix of \mathbf{g}^{LM} viz. $\boldsymbol{\Sigma}_{\mathbb{F}}^{LM}$ is related to the data covariance matrix $\boldsymbol{\Sigma}^{LM}$ by a similarity transformation

$$\boldsymbol{\Sigma}_{\mathbb{F}}^{LM} = \mathbf{M}^{LM} \boldsymbol{\Sigma}^{LM} (\mathbf{M}^{LM})^T, \quad (2.20)$$

where $\mathbf{M}^{LM} = (\mathbf{W}^T \boldsymbol{\Sigma}^{LM-1} \mathbf{W} + \lambda \boldsymbol{\Gamma})^{-1} \mathbf{W}^T \boldsymbol{\Sigma}^{LM-1}$. The confidence intervals (frequentist) given by the square root of the diagonal values of $\boldsymbol{\Sigma}_{\mathbb{F}}^{LM}$ will in general be *different* from the (Bayesian) credible intervals given by the square root of the diagonal values of $(\mathbf{H}^{LM})^{-1}$. We will present both in what follows.

3 Setup and tests

The transfer functions in eq.(2.11) were calculated using a customised version of CAMB [18] adopting the Planck best-fit cosmological model. A total of 2316 bins, evenly distributed in $\log k$ space, were used to approximate $g_{2M}(k)$ in the range from $k_{\min} \sim 7 \times 10^{-6} \text{ Mpc}^{-1}$ to $k_{\max} \sim 0.4 \text{ Mpc}^{-1}$.

Since statistical anisotropies can also be induced by the instrument itself, due to e.g. non-circular beam effects, pointing errors *etc.*, or by astrophysical foregrounds (see e.g. refs.[19, 20]), we used the most realistic simulations of the instrument and sky, viz. 999 Planck Full Focal Plane (FFP9) simulations [13] to estimate the uncertainties on the extracted BipoSH coefficients. The simulated sky maps were masked using the Planck SMICA mask (COM_Mask_CMB-confidence-Tmask-IQU-smica_1024_R2.02-full with $N_{\text{side}} = 1024$) shown in grey in Fig. 2.

The BipoSH coefficients of eq.(2.5) were then computed from the maps using our code based on HEALPix [21]. Lost power was accounted for by multiplying the coefficients by $1/f_{\text{sky}} \sim 1.176$, where f_{sky} is the available sky fraction $\sim 85\%$. First we computed the mean BipoSH coefficient $\bar{A}_q^{2M} = N_{\text{sim}}^{-1} \sum_{n=1}^{N_{\text{sim}}} A_q^{2M}(n)$ where $N_{\text{sim}} = 999$ in this case and the number in the parentheses labels the realisation. Next we computed the covariance matrix:

$$\Sigma_{qq'}^{2M} = \langle (A_q^{2M} - \bar{A}_q^{2M})(A_{q'}^{2M} - \bar{A}_{q'}^{2M}) \rangle = \frac{1}{N_{\text{sim}} - 1} \sum_{n=1}^{N_{\text{sim}}} (A_q^{2M}(n) - \bar{A}_q^{2M})(A_{q'}^{2M}(n) - \bar{A}_{q'}^{2M}), \quad (3.1)$$

and inverted this to obtain the inverse covariance matrix $\boldsymbol{\Sigma}^{2M-1}$ which was finally used to construct the likelihood:

$$-2 \log \mathcal{L}(\mathbf{g}^{2M}, \tilde{\mathbf{A}}^{2M}) = (\mathbf{W} \mathbf{g}^{2M} - \tilde{\mathbf{A}}^{2M} + \bar{\mathbf{A}}^{2M})^T \boldsymbol{\Sigma}^{2M-1} (\mathbf{W} \mathbf{g}^{2M} - \tilde{\mathbf{A}}^{2M} + \bar{\mathbf{A}}^{2M}). \quad (3.2)$$

Since the likelihood is the probability of observing the data $\tilde{\mathbf{A}}^{2M}$ in the Planck best-fit Λ CDM cosmology with an instrument that has the characteristics modelled by the FFP simulations and its foregrounds, eq.(3.2) is only valid if that is indeed what the model predicts. However since that likelihood would be very involved given the complex nature of the FFP simulations, we instead inspected the distributions of the BipoSH coefficients of the 999 realisations. The BipoSH coefficients $A_{\ell \ell+d}^{2M}$ were binned with bin size $\Delta \ell = 30$ and weighted by $\ell(\ell+1)$,

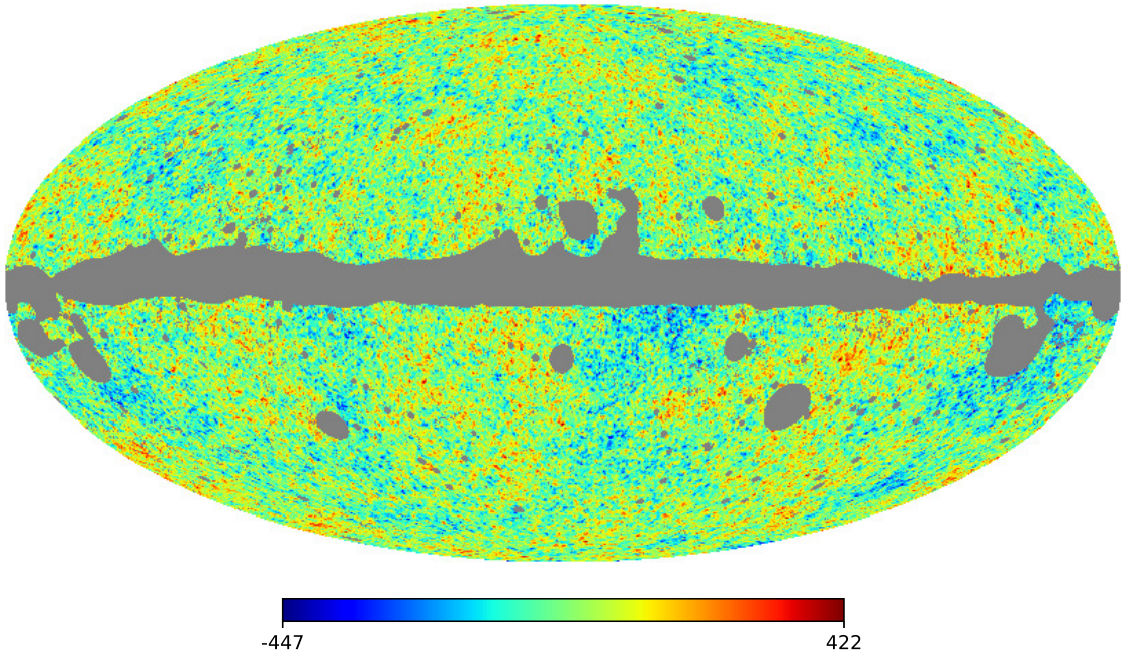


Figure 2. The masked SMICA Release 2 intensity map (the temperature fluctuations are in μK).

yielding averaged BipoSH coefficients $A_{\ell_b \ell_b+d}^{2M}$ in effective multipoles ℓ_b . Specifically, a matrix \mathbf{B} was defined with elements

$$B_{\ell_b \ell} = \frac{\ell(\ell+1)}{\sum_{\ell \in b} \ell(\ell+1)}, \quad (3.3)$$

where b is the set of multipoles in the bin. The effective multipoles are then $\ell_b = \mathbf{B}\ell$ with the effective covariance matrix $\Sigma_b^{2M} = \mathbf{B}\Sigma^{2M}\mathbf{B}^T$ and the effective BipoSH coefficients $A_{\ell_b \ell_b+d}^{2M} = \sum_{\ell} B_{\ell_b \ell} A_{\ell \ell+d}^{2M}$.

To test the normality of the distribution of BipoSH coefficients from the FFP simulations, an Anderson-Darling test [22] was performed on each distribution of $A_{\ell_b \ell_b+d}^{2M}$. The details of this test, which is sensitive to the tail of a distribution, can be found in Appendix D. The resulting p-values are shown in Fig. 3 which also shows a typical distribution.

It is seen that at 2σ significance, 52 out of 390 *i.e.* 13.3% of the distributions did not pass the Anderson-Darling test. Of these, 41 come from multipoles $\ell > 700$ as seen in Fig. 4.

An example of distribution that failed the test is shown in Fig. 5. An outlier is present that causes the distribution, which would otherwise be well modelled by a normal distribution, to fail the test. It turns out that the mask used on the skymap is responsible for most test failures. This is demonstrated by the fact that when the Anderson-Darling test is run on *unmasked* sky realisations, only 16 distributions failed, compared to 52 for the masked sky. (Of course, a certain number is expected to fail in any case as only a finite number of simulations have been run.) Despite this problem of outliers for $\ell > 700$, the Gaussian model of the likelihood seems justified and we adopt it as our likelihood.

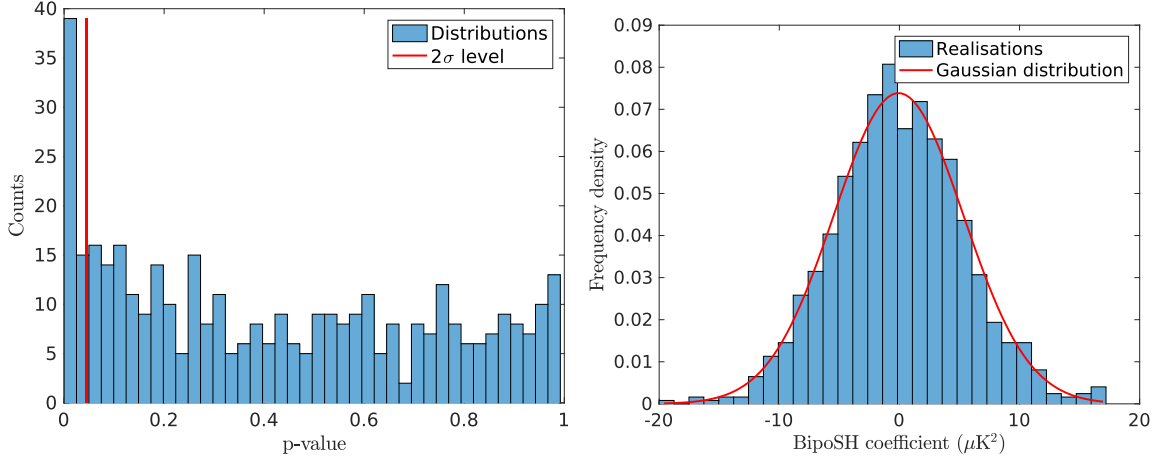


Figure 3. Tests of normality of distributions of the BipoSH coefficients $A_{\ell_b \ell_b+d}^{2M}$. In the left panel, a histogram of p-values of Anderson-Darling tests on the distributions is shown with a vertical (red) line marking the 2σ significance level. The right panel shows a histogram of 999 realisations of a particular BipoSH coefficient $A_{76 \ 76}^{2,0}$, with a Gaussian distribution superimposed.

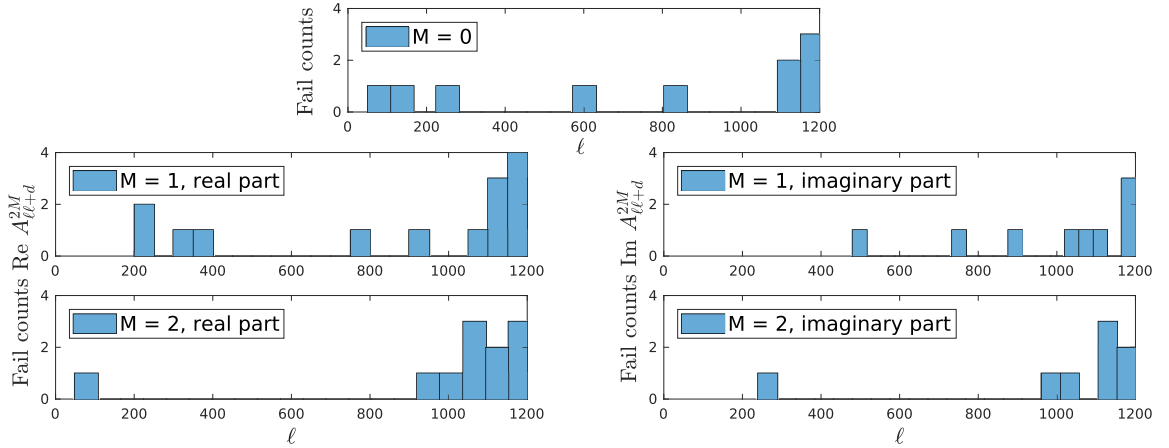


Figure 4. Counts of distributions of the BipoSH coefficients $A_{\ell \ell+d}^{2M}$ failing the Anderson-Darling test at 2σ significance level. The distributions of the real and imaginary part are shown, respectively, in the left and right panel. Note the larger count for $\ell > 1000$.

Off the diagonal of the covariance matrix, the values were found to be negligible and therefore neglected. Correlations between different values of M were also negligible.

To test our approach, the BipoSH coefficients of known quadrupole modulations were calculated. The quadrupole modulations without noise were then reconstructed from these BipoSH coefficients using eq.(2.19). The uncertainties associated with the reconstructions were taken to be those expected from an experiment that is properly modelled by the FFP simulations, including cosmic variance. The results for two different assumed modulations of $g_{20}(k)$ are shown in Fig. 6. One is a Gaussian

$$g_{20}(k) = a \exp(-(\log_{10}(k/k_0))^2/q^2), \quad (3.4)$$

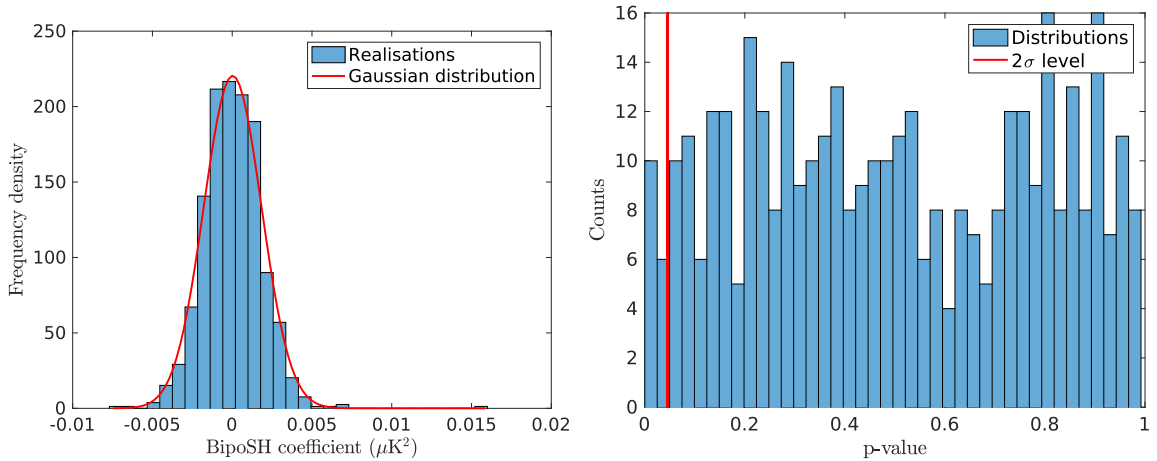


Figure 5. The left panel shows a distribution of realisations of the BipoSH coefficient $A_{1185}^{2,2}$ which fail the Anderson-Darling test due to an outlier at $\sim 0.015 \mu\text{K}^2$. In the right panel the normality test is repeated on unmasked realisations — now only 16 distributions fail the Anderson-Darling test, compared to 52 when the mask is used.

with $a = 0.5$, $k_0 = 1.26 \times 10^{-2} \text{Mpc}^{-1}$ and $q = 0.1$, while the other is a sigmoid

$$g_{20}(k) = a \exp(-(\log_{10}(k/k_0))/q) / (1 + \exp(-(\log_{10}(k/k_0))/q)), \quad (3.5)$$

with $k_0 = 2 \times 10^{-2} \text{Mpc}^{-1}$, $q = 0.2$ and $a = 0.3$. Although slight biases towards smoother spectra are visible, our reconstructions capture the features well and the credible intervals are seen to be quite distinct from zero power.

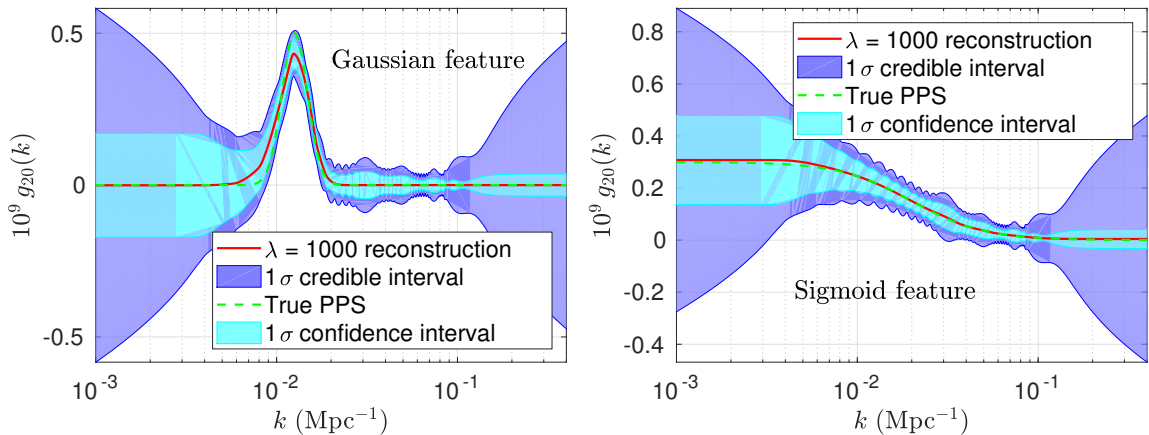


Figure 6. Reconstruction of noise-free test spectra with regularisation parameter $\lambda = 1000$. Purple bands indicate the uncertainty in the posterior probability which reflects the uncertainties associated with the experiment — cosmic variance as well as the choice of prior. Cyan bands indicate the scatter in the reconstruction due to scatter in the data. The reconstruction (full red line) matches well the true spectrum (dotted green line) and is clearly distinguishable from no power. The left and right panels show the reconstruction of a Gaussian (3.4) and sigmoid (3.5) feature respectively.

The reconstruction parameter will be biased against features if a high value of the regularisation parameter is chosen, as is evident in the Bayesian view of Tikhonov regularisation

where λ controls the roughness of the prior. The bias relative to the uncertainty is demonstrated in Fig. 7 where the Gaussian feature of Fig. 6 is reconstructed with different choices of λ . The least biased curve is the one with the smallest λ . Lowering λ , however, increases the uncertainty so that too small a value makes the reconstruction uninformative. Clearly this determines an optimal value of λ for reconstruction, as has been discussed in ref.[11].

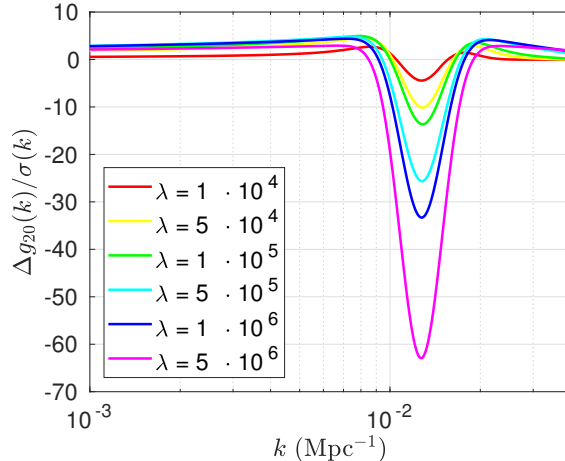


Figure 7. Bias in reconstruction of a Gaussian feature: Starting with $\lambda = 10^4$ (red) and ending with $\lambda = 5 \times 10^6$ (blue), a bias is observed with the lowest λ being least biased. The plot shows the difference between the true and the reconstructed spectrum relative to the uncertainty.

4 Results

We look for a modulation in the masked Planck SMICA Release 2 intensity map¹ (Fig. 2). The Biposh coefficients $\tilde{\mathbf{A}}^{2M}$ are calculated using eq.(2.5) for $M = 0, 1, 2$ and $d = 0, 2$ in the range $30 \leq \ell \leq 1200$. There is only a real part for $M = 0$ but $M = 1, 2$ also have imaginary parts. Fig. 8 shows the corrected (offset) data points $\tilde{\mathbf{A}}^{2M} - \bar{\mathbf{A}}^{2M}$.

4.1 Scale-independent quadrupole modulation

The best-fit *constant* spectrum $g_{2M\star}$ can be defined via the equation:²

$$g_{2M}(k) = (4\pi)^{-1/2} g_{2M\star} \mathcal{P}(k), \quad (4.1)$$

where the best-fit isotropic spectrum is taken to be $\mathcal{P}(k) = A(k/k_*)^{n_s-1}$ with $k_* = 0.05 \text{ Mpc}^{-1}$, $A = 2.198$ and $n_s = 0.9655$ (best-fit parameters from Planck TT+lowP) [23]. No regularisation is now necessary, so substituting this form into eq.(3.2), differentiating with respect to $g_{2M\star}$, and setting the expression equal to zero, we obtain the maximum-likelihood estimate:

$$\hat{g}_{2M\star} = \sqrt{4\pi} \frac{(\mathbf{W}\mathbf{p})^T \Sigma^{2M-1} (\tilde{\mathbf{A}} - \bar{\mathbf{A}})}{(\mathbf{W}\mathbf{p})^T \Sigma^{2M-1} \mathbf{W}\mathbf{p}}, \quad (4.2)$$

¹Full name is COM.CMB.IQU-smica_1024_R2.01.full with $N_{\text{side}} = 1024$.

²The numerical factor cancels the $\sqrt{4\pi}$ in eq.(1.2) and enables a direct comparison with related work [9].

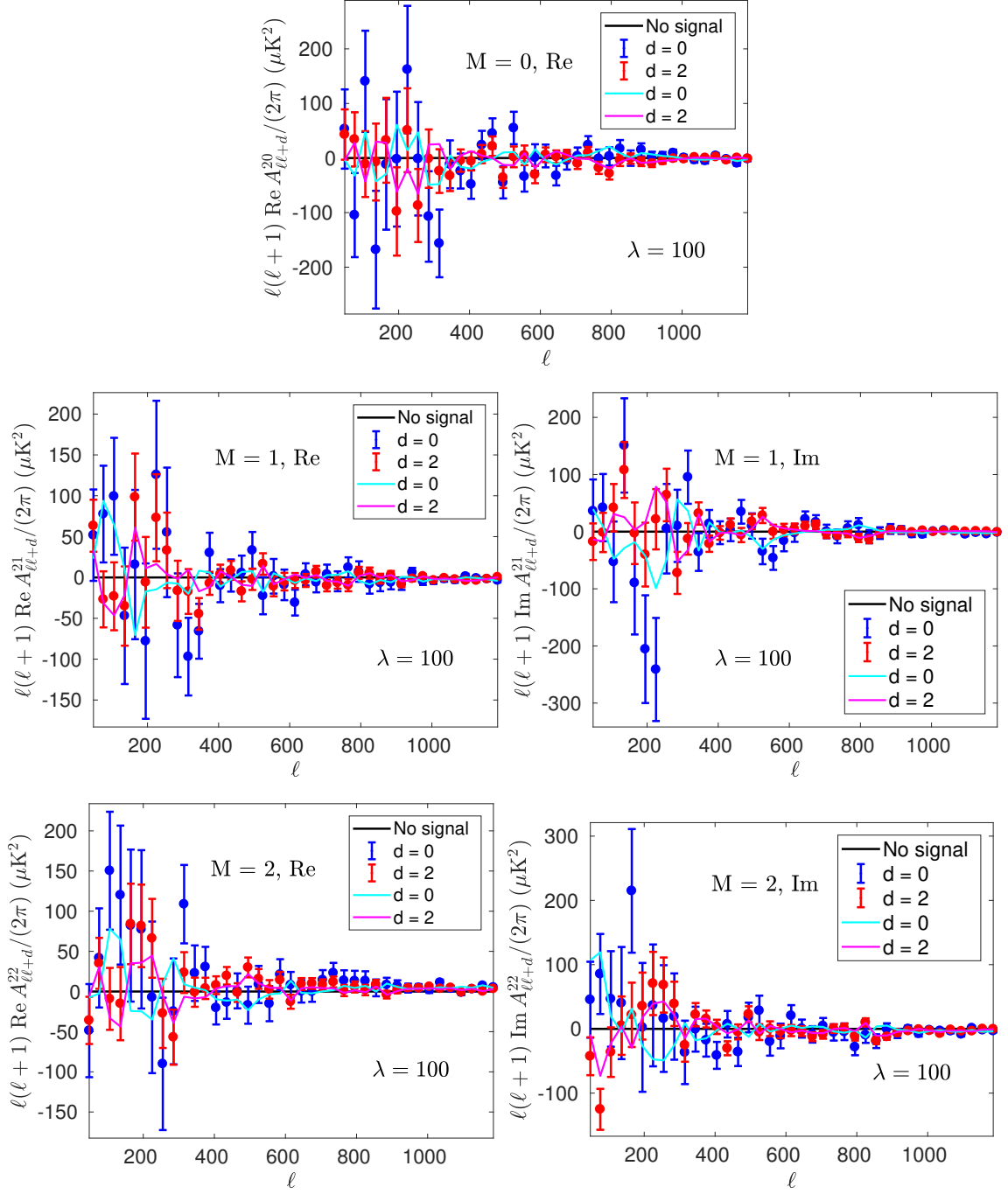


Figure 8. Real and imaginary parts of the corrected BipSH coefficients $A_{\ell, \ell+d}^{2M}$ of the masked Planck Release 2 SMICA map in bins of $\Delta\ell = 30$, with $A_{\ell, \ell}^{2M}$ ($d = 0$) in blue, and $A_{\ell, \ell+2}^{2M}$ ($d = 2$) in red. The BipSH coefficients associated with the quadrupole modulation reconstructed ($\lambda = 100$) from data (magenta lines for $d = 0$ and cyan lines for $d = 2$) are superimposed.

where \mathbf{p} is the isotropic primordial power spectrum. The uncertainty of $g_{2M\star}$ is just the inverse Hessian, *i.e.*, the inverse of the double derivative of $-\log \mathcal{L}$ with respect to $g_{2M\star}$,

which in this case is simply a number:

$$\sigma_{g_{2M\star}} = \sqrt{4\pi}((\mathbf{W}\mathbf{p})^T \Sigma^{2M-1} \mathbf{W}\mathbf{p})^{-1/2}. \quad (4.3)$$

Our results are summarised in Table 1. In summary, our search for a *constant* (scale-independent) quadrupole modulation relative to the isotropic primordial power spectrum is consistent with there being *no* such signal, consistent with earlier reports by the WMAP [17] and Planck [9] collaborations.

M	$10^2 \times \text{Re } g_{2M\star}$	$10^2 \times \text{Im } g_{2M\star}$
0	0.34 ± 0.34	
1	0.04 ± 0.21	-0.23 ± 0.21
2	0.15 ± 0.21	0.09 ± 0.21

Table 1. Results for the best-fit constant quadrupole modulation $g_{2M\star}$, eq.(4.1).

4.2 Power-law quadrupole modulations

We also tested for a power-law quadrupole modulation of the form

$$g_{2M}(k) = \frac{4\sqrt{\pi}g_*}{15} \left(\frac{k}{k_*}\right)^q \mathcal{P}(k) Y_{2M}^*(\theta, \phi) \quad (4.4)$$

where $\mathcal{P}(k)$ is the best fit isotropic spectrum and the coefficient ensures a direct comparison with ref.[10]. In real space, this corresponds to a quadrupole modulation of the form $\propto (\hat{\mathbf{k}} \cdot \hat{\mathbf{n}})^2$ where $\hat{\mathbf{n}} = (\theta, \phi)$ is a unit vector pointing in the direction of the hot spot. The posterior distribution of the parameters (g_*, θ, ϕ) was estimated using the Metropolis-Hastings algorithm with flat priors on the angles and a flat prior on g_* in the range $-10 \leq 10^2 g_* \leq 10$. We found *no evidence* of a quadrupole modulation scaling as a power law. The results are shown in Table 2. The credible intervals are such that $\sim 68.2\%$ of the probability is

q	-2	-1	0	1	2
$10^2 g_*$	$-0.03^{+0.22}_{-0.23}$	$0.11^{+0.54}_{-0.57}$	$0.10^{+0.40}_{-0.41}$	$0.00^{+0.25}_{-0.25}$	$-0.05^{+0.19}_{-0.18}$

Table 2. Results for the best-fit power-law quadrupole modulations of the form of eq.(4.4) for different power law indices.

contained in the quoted ranges. The posterior distribution of g_* found after marginalising over the directions θ, ϕ is shown in Fig. 9 for the case of $q = 0$. A Mollweide projection of the *posterior distribution* of the direction (θ, ϕ) for each value of the power q is shown in Fig. 20. Note that directions are poorly determined.

Similarly, eq.(4.1) can be generalised to include a power-law quadrupole modulation:

$$g_{2M}(k) = (4\pi)^{-1/2} g_{2M\star} (k/k_*)^q \mathcal{P}(k), \quad (4.5)$$

with power q and amplitude $g_{2M\star}$. Unlike the previously considered form (4.4), this allows for the most general quadrupole power law modulation which means that the directions of the two dipoles that a quadrupole can be factorised into need *not* coincide. The maximum

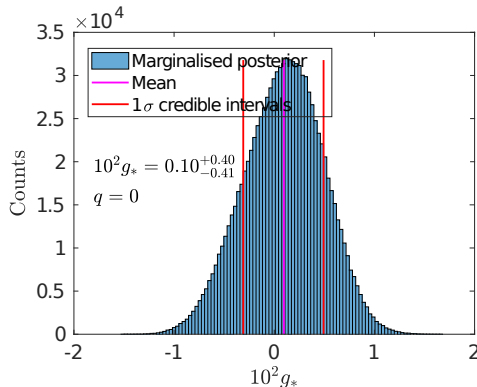


Figure 9. Metropolis-Hastings sampled posterior distribution of $10^2 g_*$ assuming a flat prior on $-10 \leq 10^2 g_* \leq 10$ and marginalising over the angles θ, ϕ . Magenta line marks the mean and the red lines indicate the region that includes $\sim 68.2\%$ of the probability.

likelihood amplitudes and uncertainties of such modulations are given by the same expressions as those for the constant quadrupole modulation *upon* replacing the discretised version of $\mathcal{P}(k)$ (*i.e.*, \mathbf{p} in eqs.(4.2) and (4.3)) with a discretised version of $\mathcal{P}(k)(k/k_*)^q$. The results are shown in Table 6 and Figure 22. Our estimates are consistent with there being *no* power law quadrupole modulation. This will be made precise in Section 5.

A quadrupole is described by two directions, $\hat{\mathbf{n}}_1$ and $\hat{\mathbf{n}}_2$, and an amplitude g_A and is of the form $g_A(\hat{\mathbf{k}} \cdot \hat{\mathbf{n}}_1)(\hat{\mathbf{k}} \cdot \hat{\mathbf{n}}_2)$ where $\hat{\mathbf{k}} = (\theta, \phi)$. The relation between the quadrupole modulations g_{2M} and the direction is found by decomposing this form into spherical harmonics

$$g_{2M} = g_A \int d\Omega (\hat{\mathbf{k}} \cdot \hat{\mathbf{n}}_1)(\hat{\mathbf{k}} \cdot \hat{\mathbf{n}}_2) Y_{2M}^*(\theta, \phi). \quad (4.6)$$

The best-fit quadrupole modulations for the different powers q are displayed in Fig. 22, although they are not particularly informative as there are large uncertainties in the directions $\hat{\mathbf{n}}_1$ and $\hat{\mathbf{n}}_2$ (as seen for the case of the constant quadrupole modulation $q = 0$ in Fig. 21).

4.3 Non-parametric quadrupole modulations

We now present *new* results concerning a possible *scale-dependent* (non-parametric) quadrupole modulation of the primordial power spectrum. The quadrupole modulation reconstructed using eq.(2.19) from the masked Planck SMICA Release 2 temperature map, with uncertainties modelled by the masked FFP simulations, is shown in Fig. 10 for $\lambda = 100$ and in Fig. 12 for $\lambda = 5000$. Plots for other choices of λ are shown in Appendix B.

The non-parametric reconstructions suggest the presence of a feature at $k \sim 0.006 \text{ Mpc}^{-1}$ in $\text{Im } g_{22}$ with respect to both Bayesian and frequentist uncertainties. The dominant contributions to this feature are from the BipoSH coefficients $\text{Im } A_{74}^{22}$ and $\text{Im } A_{76}^{22}$ which are themselves bins of BipoSH coefficients in the multipole range $60 \leq \ell \leq 90$.

We now proceed to investigate the direction of this possible feature. When fitting the quadrupole modulation of eq.(4.6) to the data over a limited wave number range, $0.005 \leq k/\text{Mpc}^{-1} \leq 0.008$, assuming just one direction $\hat{\mathbf{n}}_1 = \hat{\mathbf{n}}_2$ and a constant amplitude g_A , we find that the posterior probability distribution of the direction is bimodal, but that a ‘hot’ ($g_A > 0$) quadrupole modulation is preferred. Histograms of the posterior distribution of

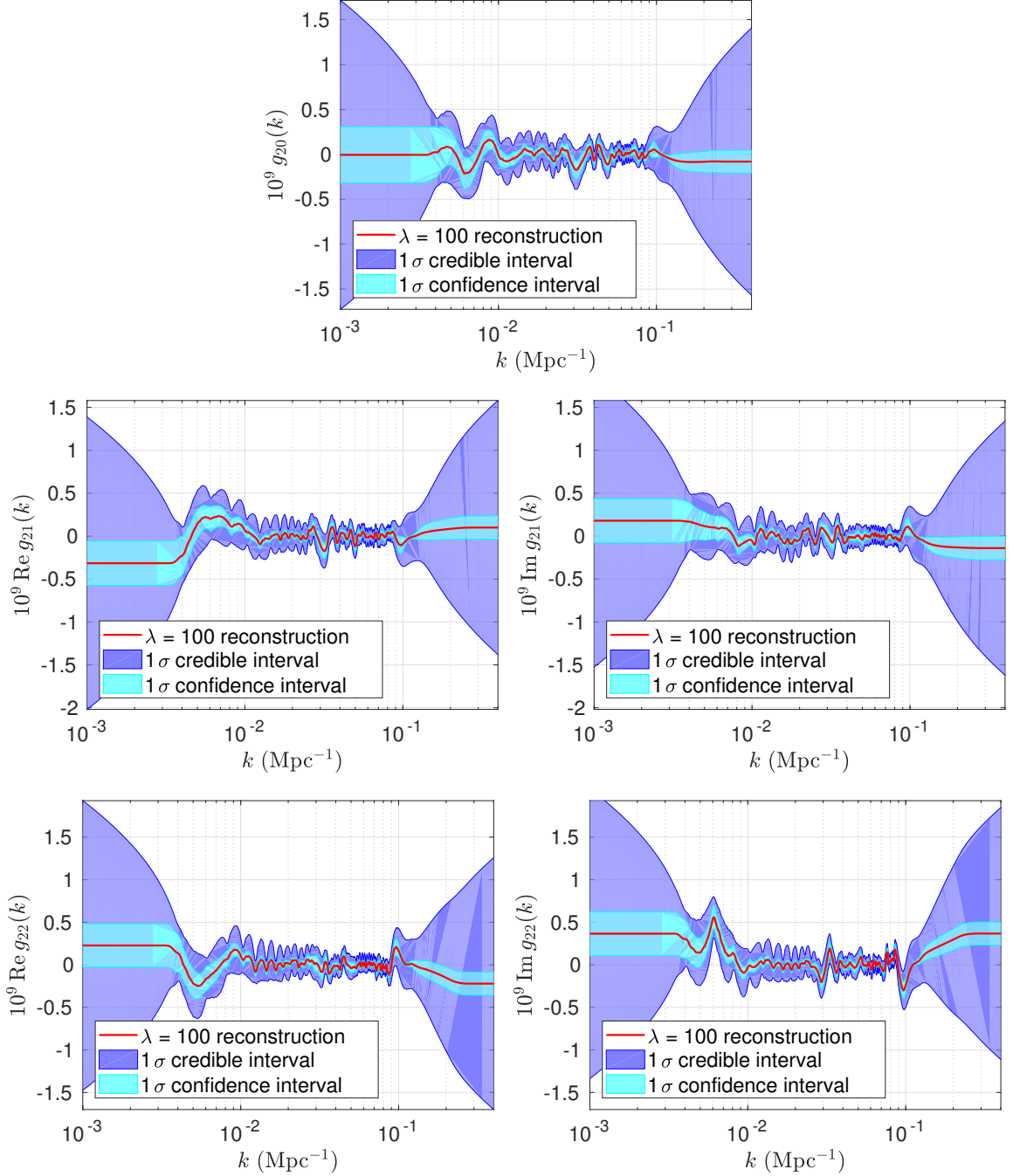


Figure 10. Reconstruction (full red line) of the quadrupole modulation from masked and binned ($\Delta\ell = 30$) Planck Release 2 SMICA temperature data in the multipole range $30 \leq \ell \leq 1200$. Purple bands and cyan bands indicate the 1σ credible intervals and 1σ confidence intervals, respectively. The regularisation parameter was set to $\lambda = 100$. Note the feature at $k \sim 6 \times 10^{-3} \text{ Mpc}^{-1}$ in $\text{Im } g_{22}$.

the direction for both cases are shown in Fig. 11. Details of the directions are provided in Table 3 where angular distances to the CMB dipole (interpreted as a Doppler boost) and the hemispherical asymmetry [24], as determined in ref.[9], are calculated.

In both cases, the direction of the quadrupole modulation is *perpendicular* to that of

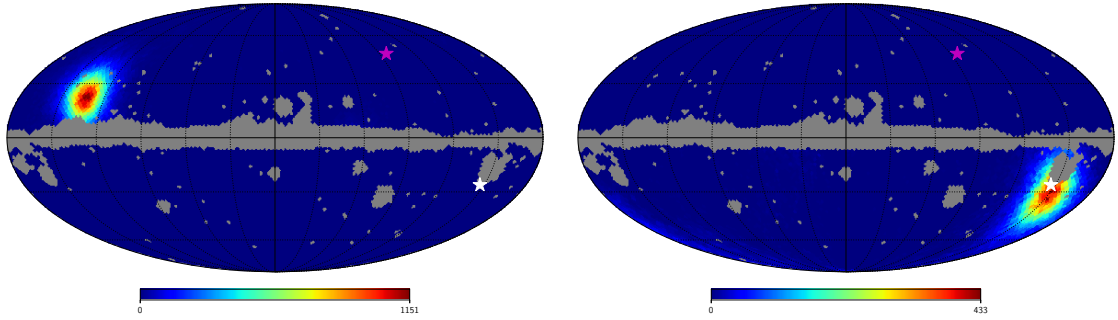


Figure 11. Histograms of the posterior distribution of the direction $\hat{\mathbf{n}}$ for the case of a hot ($10^9 g_A = 0.51 \pm 0.16$) constant quadrupole modulation (left panel) and a cold ($10^9 g_A = -0.42 \pm 0.18$) modulation (right panel) in the wave number range $0.005 \leq k/\text{Mpc}^{-1} \leq 0.008$. The SMICA mask (in grey) is superimposed for comparison. The magenta and white stars indicate the directions of the CMB dipole and the hemispherical asymmetry, respectively.

For $k = 0.005\text{-}0.008 \text{ Mpc}^{-1}$:		Angular distances to:	
Amp. $10^9 g_A$	Direction (l, b)	CMB dipole ($264^\circ, 48^\circ$)	Hemisp. asym. ($213^\circ, -26^\circ$)
0.51 ± 0.16	$(136^{+13}_{-12}, 22^{+10}_{-11})$	96°	89°
-0.42 ± 0.18	$(212^{+13}_{-12}, -30^{+14}_{-15})$	91°	4°

Table 3. Details of the two modes of the posterior distribution of the quadrupole modulation direction shown in Fig. 11. The first mode is for the case of a hot modulation. Angular distances to the directions of the CMB dipole and the hemispherical asymmetry are also indicated.

the CMB dipole. In the case of a hot quadrupole modulation ($g_A > 0$), the direction of the quadrupole modulation is perpendicular to that of the hemispherical asymmetry, whereas in the case of a cold quadrupole modulation, it is parallel. It is quite unexpected that the direction of the quadrupole modulation should be related to that of either the CMB dipole or the hemispherical asymmetry.

We will relegate the discussion of features and their statistical significance to the next section where all five components will be compressed to a single amplitude $g_2(k)$.

5 Statistical significance of a quadrupole modulation

5.1 Power law quadrupole modulations

To test the statistical significance of power-law quadrupole modulations

$$g_{2M}(k) = (4\pi)^{-1/2} g_{2M\star} (k/k_\star)^q \mathcal{P}(k) \quad (5.1)$$

we calculate the overall amplitude

$$g_2 = \sqrt{\frac{1}{5} \sum_M |g_{2M\star}|^2} \quad (5.2)$$

for the components $\hat{g}_{2M\star}$ that best fit the data and compare it with the estimates of g_2 calculated from 10^4 realisations of only noise that is modelled by the covariance matrix Σ^{2M}

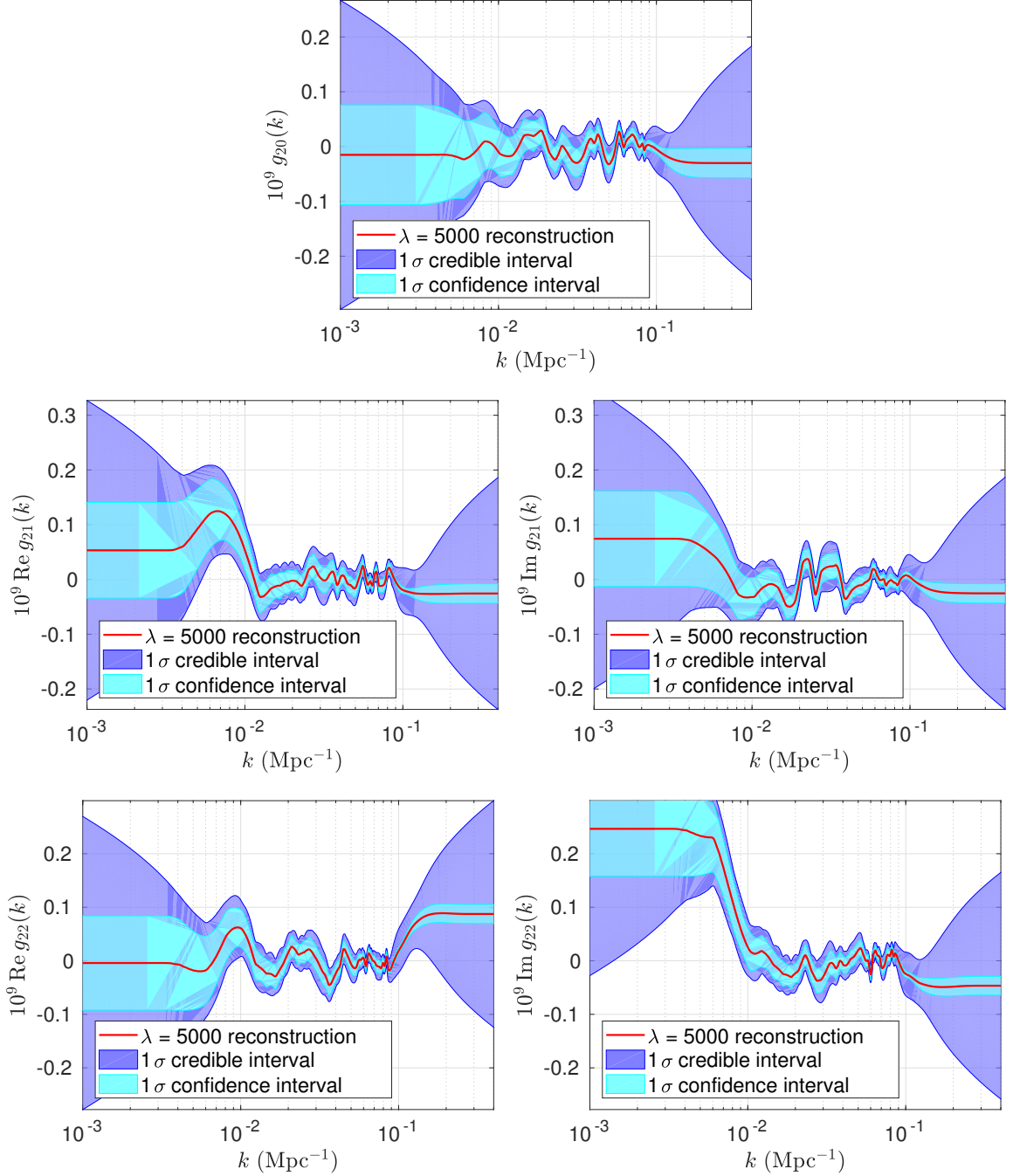


Figure 12. Reconstruction (full red line) with credible intervals (purple band) and confidence intervals (cyan band) for $\lambda = 5000$.

derived from the FFP simulations. Each realisation is a set of BipoSH coefficients \mathbf{A}^{2M} from which $g_{2M\star}$ can be deduced using eq.(4.2). These are then used to compute g_2 . The p-value is equal to the fraction of realisations with g_2 greater than or equal to the value \hat{g}_2 obtained from data and is shown in Table 4. It is clear that the best-fit values of g_2 we have obtained from data are consistent with there being *no* signal.

q	-2	-1	0	1	2
p-value	0.40	0.59	0.68	0.66	0.33

Table 4. P-value test of g_2 (5.2) calculated for power law quadrupole modulations from data and compared with 10^4 noise realisations.

5.2 Non-parametric quadrupole modulations

We repeat the same procedure for the reconstructions $g_{2M}(k)$ from data, calculating

$$g_2(k) = \sqrt{\frac{1}{5} \sum_M |g_{2M}(k)|^2} \quad (5.3)$$

for the ($\lambda = 100$) reconstruction from data and for the ($\lambda = 100$) reconstructions from 10^4 realisations of only noise. The results are shown in Fig. 13, where on the right, the mean of the noise realisations, $\bar{g}_2(k) = N^{-1} \sum_{j=N} g_{2,j}(k)$, has been subtracted from $g_2(k)$. Using the noise realisations, a covariance matrix for $g_2(k)$ was constructed:

$$\Sigma_{g_2 k k'} = \frac{1}{N-1} \sum_{j=1}^N (g_{2,j}(k) - \bar{g}_2(k))(g_{2,j}(k') - \bar{g}_2(k')), \quad (5.4)$$

the square root of whose diagonal values have been used as standard deviations in the plots of Fig. 13. The amplitude $g_2(k)$ suggests the presence of features at 0.006, 0.033, 0.061, 0.0826, 0.086, 0.096 Mpc^{-1} . However, a test of the global significance should be made. For that, the

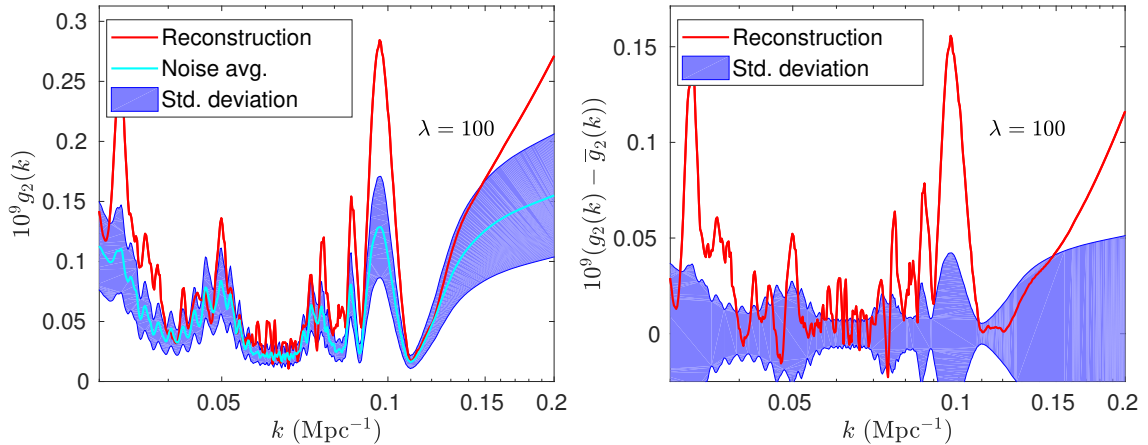


Figure 13. The left panel shows the amplitude $g_2(k)$ for the reconstruction from data (red line) and its mean (cyan line) and standard deviation (purple band) of $g_2(k)$ for the noise realisations. In the right panel, this mean $\bar{g}_2(k)$ has been subtracted from the $g_2(k)$ reconstructed from data.

constructed covariance matrix was inverted and used in a χ^2 statistic:

$$T_{g_2}(g_2(k)) = (\mathbf{g}_2 - \bar{\mathbf{g}}_2)^T \Sigma_{g_2}^{-1} (\mathbf{g}_2 - \bar{\mathbf{g}}_2) \quad (5.5)$$

where the bold notation has been used to suppress the wave number indices. Strictly speaking, the covariance matrix is not invertible and so a pseudoinverse must be used instead. This

statistic was calculated for the noise realisations as well as the reconstruction from data and a p-value was thus derived. The results are shown in Fig. 14 where the right panel shows the results of the p-value test for a region of wave numbers limited to $0.008 \leq k/\text{Mpc}^{-1} \leq 0.074$. The p-values translate to 2.48σ and 2.21σ significance levels, respectively. These are quite

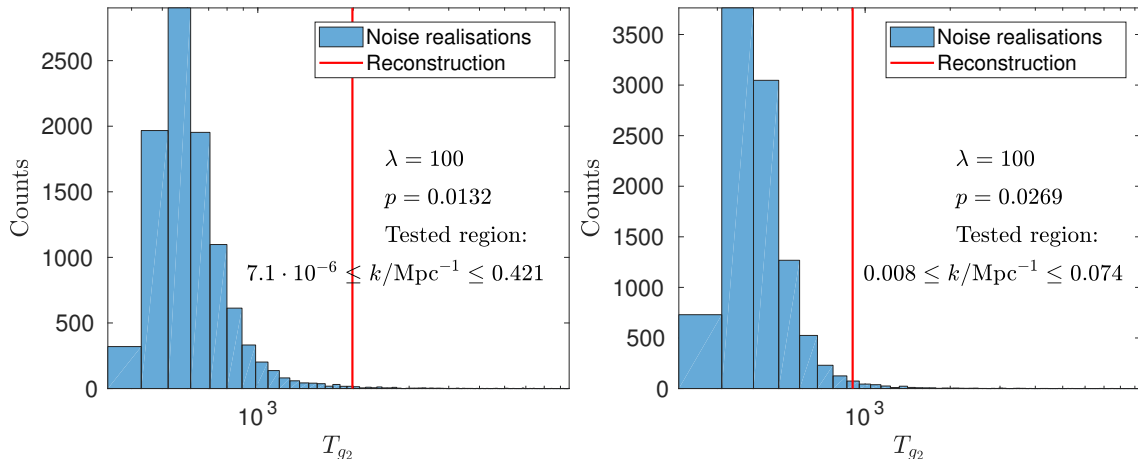


Figure 14. P-value test using T_{g_2} . The distribution of T_{g_2} for noise realisations and the value of T_{g_2} for the reconstruction from data (red line). The right panel shows the same test, but for a more restricted range of wave numbers.

marginal. However, we shall now argue that another test statistic should be adopted that is more sensitive and under better theoretical control. Though T_{g_2} is based on the amplitude g_2 which is rotationally invariant, it is not the case that all components g_{2M} are equally uncertain since the covariance matrices Σ^{2M} are not equal to one another, and so equal statistical weight should not be given to all components. Since the statistic is based on the amplitude, it is insensitive to the direction. If a certain direction is systematically singled out across k , but with a small amplitude, that will count no more than randomly oriented quadrupole modulations across k . Also, we do not have good theoretical control over the test statistic T_{g_2} . It can be seen in both panels of Fig. 14 that the possible values of T_{g_2} for the noise realisations, though peak around 500, still appear at values up to 10^4 .

We shall now present a test statistic which addresses these issues. We propose to construct a χ^2 statistic using the frequentist covariance matrix

$$T(g_{2M}) = \mathbf{g}_{2M}^T \Sigma_{\text{F}}^{2M-1} \mathbf{g}_{2M}. \quad (5.6)$$

Strictly speaking, the inverse of the frequentist covariance matrix does not exist, but its pseudoinverse does. We have proven in Appendix C that, using the pseudoinverse, $T(g_{2M})$ is distributed according to a χ^2 distribution with degrees of freedom equal to the rank of the pseudoinverse covariance matrix which should equal the rank of the original covariance matrix of the data, which is 78 per component of g_{2M} , or, 390 for all five (three real and two imaginary) components considered together. Therefore we consider the test statistic

$$T = \sum_{\text{Re,Im}, M \geq 0} \mathbf{g}_{2M}^T \Sigma_{\text{F}}^{2M-1} \mathbf{g}_{2M} \quad (5.7)$$

which, when using all data, should have a χ^2 distribution with 390 degrees of freedom.

First we illustrate in the left panel of Fig. 15 that the frequentist covariance matrix corresponds to the standard deviation of reconstructed spectra of noise realisations. The standard deviation of the noise realisations of $\text{Im } g_{22}$ defining the purple band is exactly bounded by the magenta line which is the square root of the diagonal entries of Σ_F which give the 1σ confidence intervals. The results for the p-value tests using $T(g_{2M})$ are shown on the right panel of Fig. 15 where it is seen that the quadrupole modulation reconstructed from data is quite rare. No noise realisations were found to have as extreme a value of T . In fact, the theoretical distribution is able to tell us the answer: $p = F_{390}(528) \sim 3.6 \times 10^{-6} \sim 4.63\sigma$ where F_{390} is the cumulative distribution function of χ_{390}^2 . By restricting the wave number range to $0.008 \leq k/\text{Mpc}^{-1} \leq 0.074$, we find that the reconstruction from data is made more likely. The results of the p-value tests are shown in Fig. 16. For the restricted range $0.008 \leq k/\text{Mpc}^{-1} \leq 0.074$, the p-value is 0.0066, corresponding to 2.72σ significance. Hence even after cutting the data, the spectrum is unlikely to have been a realisation of noise only. The g_{22} component seems to be contributing the most to the deviation. This is in accordance with our expectation that T is the more sensitive test statistic as it is made of a component by component test, and here it is the component g_{22} that is the cause of the discrepancy.

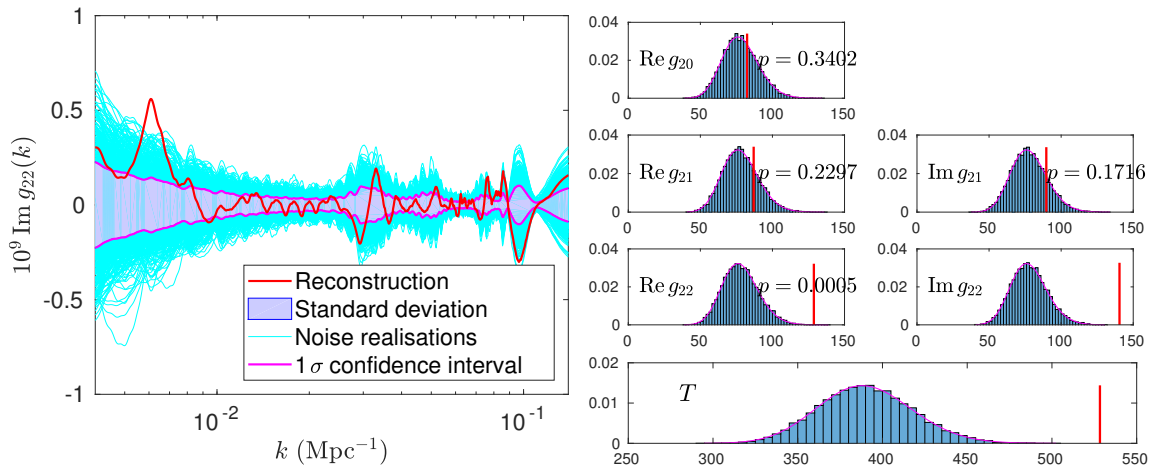


Figure 15. The left panel shows the noise realisations (thin cyan lines), their standard deviation (purple band) as well as the reconstruction from data (red line). The 1σ confidence interval (magenta lines) derived from the frequentist covariance matrix exactly matches the standard deviation. The right panel shows the results of the p-value test of $T(g_{2M})$ and the final test statistic T with a red line indicating their values for the reconstruction from data. The purple lines are the theoretical distributions of the test statistic.

6 Summary and conclusion

We have described a method for reconstructing a direction- *and* scale-dependent modulation of the primordial power spectrum, using Tikhonov regularisation and bipolar spherical harmonics coefficients. The BipoSH coefficients capture the statistical anisotropy of a CMB map and Tikhonov regularisation can then be used to infer the direction-dependent primordial power spectrum responsible. The uncertainties were estimated using the Planck Full Focal Plane (FFP9) simulations and a simplified Gaussian likelihood was constructed. The method was then used on the Planck Release 2 SMICA temperature map for the multipole range $30 \leq \ell \leq 1200$, binned with $\Delta\ell = 30$.

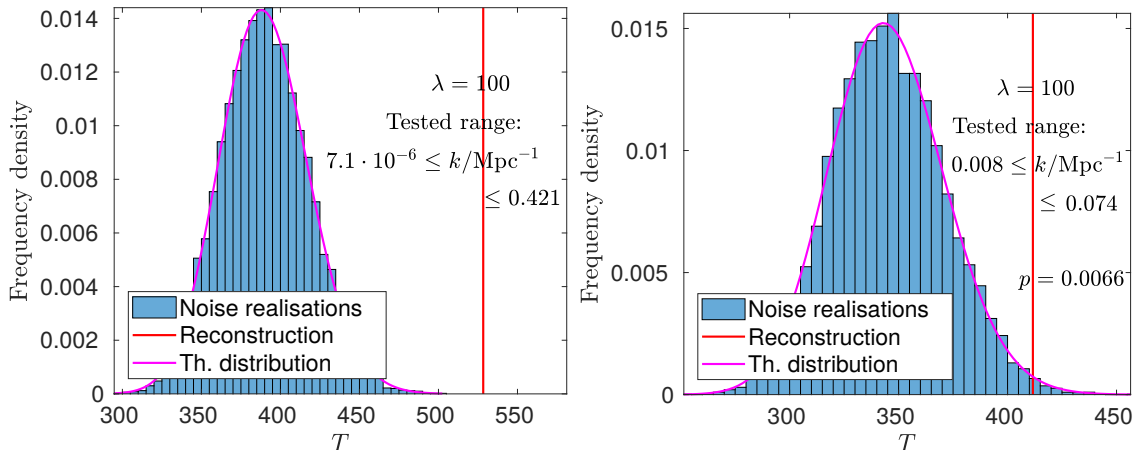


Figure 16. P-value tests of T for the full range of wave numbers (left panel) and a more limited range (right panel). The value of T for the reconstruction from data is indicated with a red line.

Consistent with previous work we find no indication of a constant quadrupole modulation nor one scaling with wave number as a power law. However our non-parametric reconstruction suggests spectral features at 0.006, 0.033, 0.061, 0.0826, 0.086, and 0.096 Mpc^{-1} .

Guided by the feature at 0.006 Mpc^{-1} , the dominant contribution to which comes from multipoles $60 \leq \ell \leq 90$, we fit a constant quadrupole modulation to data in the restricted wave number range $0.005 \leq k/\text{Mpc}^{-1} \leq 0.008$ and find that the preferred direction of this modulation is perpendicular to the CMB dipole and aligned with that of the well-known hemispherical asymmetry. This is an unexpected result that merits further investigation.

In order to assess the global significance, we construct two test statistics to evaluate reconstructions from data against reconstructions of noise only. With a test statistic sensitive only to the amplitude, we find the reconstruction from data to be unusual at 2.48σ significance for the full wave number range, and 2.21σ when we only consider intermediate wave numbers $0.008 \leq k/\text{Mpc}^{-1} \leq 0.074$. With the test statistic we have argued to be the more appropriate one which is sensitive to a preferred direction as well, the significance increases to 4.63σ and 2.72σ , respectively, for the full and intermediate range of wave numbers.

Our method goes beyond previous work in allowing for non-parametric scale-dependence in a possible quadrupolar modulation and can be easily generalised to include higher order modulations as well. The binning in multipoles and restriction to $\ell > 30$ can be avoided by constructing a non-Gaussian likelihood which makes full use of the Planck data and simulations. Other data sets such as polarisation, large-scale structure and future 21-cm line observations can also be incorporated. An immediate suggestion for future work would be to consider different Planck maps, and also consider different masks.

Acknowledgments

We thank Jeppe Trøst Nielsen for helpful suggestions and Sebastian von Hausegger, Hao Liu, Pavel Naselsky, Benjamin Wandelt, Guilhem Lavaux, Roya Mohayaee, Chris Pethick and Andrew Jackson for discussions. AD and SS were supported by the Danish National Research Foundation. SM acknowledges support from the Simons Foundation, the Labex ILP (ANR-10-LABX-63) part of the IDEX SUPER, the Agence Nationale de la Recherche as

part of the programme Investissements d’avenir (ANR-11-IDEX-0004-02), and hospitality at the Niels Bohr Institute where this work was initiated. SM also acknowledges the NERSC and Planck collaboration for providing the FFP simulations and auxiliary files.

References

- [1] L. H. Ford, *Inflation driven by a vector field*, *Phys. Rev.* **D40** (1989) 967.
- [2] A. E. Gumrukcuoglu, C. R. Contaldi and M. Peloso, *CMB anomalies from relic anisotropy*, in *Proceedings, 11th Marcel Grossmann Meeting, MG11, Berlin, Germany, July 23-29, 2006. Pt. A-C*, pp. 1641–1646, 2006. [astro-ph/0608405](#). DOI.
- [3] L. Ackerman, S. M. Carroll and M. B. Wise, *Imprints of a Primordial Preferred Direction on the Microwave Background*, *Phys. Rev.* **D75** (2007) 083502, [[astro-ph/0701357](#)].
- [4] B. Himmetoglu, C. R. Contaldi and M. Peloso, *Instability of anisotropic cosmological solutions supported by vector fields*, *Phys. Rev. Lett.* **102** (2009) 111301, [[0809.2779](#)].
- [5] B. Himmetoglu, C. R. Contaldi and M. Peloso, *Instability of the ACW model, and problems with massive vectors during inflation*, *Phys. Rev.* **D79** (2009) 063517, [[0812.1231](#)].
- [6] M.-a. Watanabe, S. Kanno and J. Soda, *Inflationary universe with anisotropic hair*, *Phys. Rev. Lett.* **102** (2009) 191302, [[0902.2833](#)].
- [7] A. L. Erickcek, M. Kamionkowski and S. M. Carroll, *A Hemispherical Power Asymmetry from Inflation*, *Phys. Rev.* **D78** (2008) 123520, [[0806.0377](#)].
- [8] A. R. Pullen and M. Kamionkowski, *Cosmic Microwave Background Statistics for a Direction-Dependent Primordial Power Spectrum*, *Phys. Rev.* **D76** (2007) 103529, [[0709.1144](#)].
- [9] PLANCK collaboration, P. A. R. Ade et al., *Planck 2015 results. XVI. Isotropy and statistics of the CMB*, *Astron. Astrophys.* **594** (2016) A16, [[1506.07135](#)].
- [10] PLANCK collaboration, P. A. R. Ade et al., *Planck 2015 results. XX. Constraints on inflation*, *Astron. Astrophys.* **594** (2016) A20, [[1502.02114](#)].
- [11] P. Hunt and S. Sarkar, *Reconstruction of the primordial power spectrum of curvature perturbations using multiple data sets*, *JCAP* **1401** (2014) 025, [[1308.2317](#)].
- [12] P. Hunt and S. Sarkar, *Search for features in the spectrum of primordial perturbations using Planck and other datasets*, *JCAP* **1512** (2015) 052, [[1510.03338](#)].
- [13] PLANCK collaboration, P. A. R. Ade et al., *Planck 2015 results. XII. Full Focal Plane simulations*, *Astron. Astrophys.* **594** (2016) A12, [[1509.06348](#)].
- [14] A. Hajian and T. Souradeep, *Measuring statistical isotropy of the CMB anisotropy*, *Astrophys. J.* **597** (2003) L5–L8, [[astro-ph/0308001](#)].
- [15] A. Hajian and T. Souradeep, *The Cosmic microwave background bipolar power spectrum: Basic formalism and applications*, [astro-ph/0501001](#).
- [16] L. G. Book, M. Kamionkowski and T. Souradeep, *Odd-Parity Bipolar Spherical Harmonics*, *Phys. Rev.* **D85** (2012) 023010, [[1109.2910](#)].
- [17] C. L. Bennett et al., *Seven-year Wilkinson Microwave Anisotropy Probe (WMAP) observations: Are there cosmic microwave background anomalies?*, *Astrophys. J. Suppl.* **192** (2011) 17, [[1001.4758](#)].
- [18] A. Lewis and S. Bridle, *Cosmological parameters from CMB and other data: A Monte Carlo approach*, *Phys. Rev.* **D66** (2002) 103511, [[astro-ph/0205436](#)].
- [19] S. Das, S. Mitra, A. Rotti, N. Pant and T. Souradeep, *Statistical isotropy violation in WMAP CMB maps resulting from non-circular beams*, *Astron. Astrophys.* **591** (2016) A97, [[1401.7757](#)].

- [20] J. Kim and E. Komatsu, *Limits on anisotropic inflation from the Planck data*, *Phys. Rev.* **D88** (2013) 101301, [[1310.1605](#)].
- [21] K. M. Gorski, E. Hivon, A. J. Banday, B. D. Wandelt, F. K. Hansen, M. Reinecke et al., *HEALPix - A Framework for high resolution discretization, and fast analysis of data distributed on the sphere*, *Astrophys. J.* **622** (2005) 759–771, [[astro-ph/0409513](#)].
- [22] T. W. Anderson and D. A. Darling, *A test of goodness of fit*, *Journal of the American Statistical Association* **49** (1954) 765–769.
- [23] PLANCK collaboration, P. A. R. Ade et al., *Planck 2015 results. XIII. Cosmological parameters*, *Astron. Astrophys.* **594** (2016) A13, [[1502.01589](#)].
- [24] H. K. Eriksen, F. K. Hansen, A. J. Banday, K. M. Gorski and P. B. Lilje, *Asymmetries in the Cosmic Microwave Background anisotropy field*, *Astrophys. J.* **605** (2004) 14–20, [[astro-ph/0307507](#)].
- [25] M. A. Stephens, *The Anderson-Darling statistic*, tech. rep., Department of Statistics, Stanford University, 1979.

A Relating quadrupole modulations to BipoSH coefficients

We investigate in detail the relation between a given quadrupole modulation $g_{LM}(k)$ and the BipoSH coefficient $A_{\ell\ell'}^{LM}$. In linear theory, there is a simple relation between the temperature perturbation $\Delta T/T_0$ in the direction $\hat{\mathbf{n}}$ at the position \mathbf{x} at time t and the curvature perturbation $\mathcal{R}(\mathbf{k})$, *viz.*

$$\frac{\Delta T}{T_0}(\mathbf{x}, \hat{\mathbf{n}}, t) = \int \frac{d^3k}{(2\pi)^3} \exp(i\mathbf{k} \cdot \mathbf{x}) \Theta(\mathbf{k}, \hat{\mathbf{n}}, t) \mathcal{R}(\mathbf{k}), \quad (\text{A.1})$$

where $\Theta(\mathbf{k}, \hat{\mathbf{n}}, t)$ is the transfer function. Assuming that the cosmological evolution itself does not induce any anisotropy, the transfer function can depend only on $\hat{\mathbf{k}} \cdot \hat{\mathbf{n}}$ which has value between -1 and 1. It can therefore be expressed in terms of Legendre polynomials $P_\ell(\hat{\mathbf{k}} \cdot \hat{\mathbf{n}})$ which are complete on the interval $[-1, 1]$, with coefficients Θ_ℓ :

$$\Theta(\mathbf{k}, \hat{\mathbf{n}}, t) = \sum_{\ell} (-i)^\ell (2\ell + 1) \Theta_\ell(k, t) P_\ell(\hat{\mathbf{k}} \cdot \hat{\mathbf{n}}). \quad (\text{A.2})$$

The Legendre polynomials may be expressed as spherical harmonics:

$$P_\ell(\hat{\mathbf{k}} \cdot \hat{\mathbf{n}}) = \frac{4\pi}{2\ell + 1} \sum_{m=-\ell}^{\ell} Y_{\ell m}(\hat{\mathbf{k}}) Y_{\ell m}^*(\hat{\mathbf{n}}), \quad (\text{A.3})$$

so that:

$$\Theta(\mathbf{k}, \hat{\mathbf{n}}, t) = 4\pi \sum_{\ell m} (-i)^\ell \Theta_\ell(k, t) Y_{\ell m}(\hat{\mathbf{k}}) Y_{\ell m}^*(\hat{\mathbf{n}}). \quad (\text{A.4})$$

The central object is the angular correlation function

$$C(\hat{\mathbf{n}}, \hat{\mathbf{n}}') = \left\langle \frac{\Delta T}{T_0}(\mathbf{x}, \hat{\mathbf{n}}, t) \frac{\Delta T}{T_0}(\mathbf{x}, \hat{\mathbf{n}}', t) \right\rangle, \quad (\text{A.5})$$

which can be re-expressed using (A.4):

$$C(\hat{\mathbf{n}}, \hat{\mathbf{n}}') = \sum_{\ell m} \sum_{\ell' m'} (4\pi)^2 (-i)^{\ell+\ell'} Y_{\ell m}(\hat{\mathbf{n}}) Y_{\ell' m'}(\hat{\mathbf{n}}') \int \frac{d^3 k}{(2\pi)^3} \int \frac{d^3 k'}{(2\pi)^3} e^{i(\mathbf{k}+\mathbf{k}')\cdot\mathbf{x}} \Theta_{\ell}(k, t) \Theta_{\ell'}(k', t) Y_{\ell m}^*(\hat{\mathbf{k}}) Y_{\ell' m'}^*(\hat{\mathbf{k}}') \langle \mathcal{R}(\mathbf{k}) \mathcal{R}(\mathbf{k}') \rangle. \quad (\text{A.6})$$

Now, we know that

$$\langle \mathcal{R}(\mathbf{k}) \mathcal{R}(\mathbf{k}') \rangle = (2\pi)^3 \delta^{(3)}(\mathbf{k} + \mathbf{k}') P(\mathbf{k}) \quad (\text{A.7})$$

$$= (2\pi)^3 \delta^{(3)}(\mathbf{k} + \mathbf{k}') \frac{2\pi^2}{k^3} \mathcal{P}(\mathbf{k}) \quad (\text{A.8})$$

$$= (2\pi)^3 \delta^{(3)}(\mathbf{k} + \mathbf{k}') \frac{2\pi^2}{k^3} \sqrt{4\pi} \sum_{LM} g_{LM}(k) Y_{LM}(\hat{\mathbf{k}}), \quad (\text{A.9})$$

so, replacing $\langle \mathcal{R}(\mathbf{k}) \mathcal{R}(\mathbf{k}') \rangle$, we get

$$C(\hat{\mathbf{n}}, \hat{\mathbf{n}}') = \sqrt{4\pi} \sum_{\ell m} \sum_{\ell' m'} (4\pi)^2 (-i)^{\ell+\ell'} Y_{\ell m}(\hat{\mathbf{n}}) Y_{\ell' m'}(\hat{\mathbf{n}}') \int \frac{d^3 k}{(2\pi)^3} \int \frac{d^3 k'}{(2\pi)^3} e^{i(\mathbf{k}+\mathbf{k}')\cdot\mathbf{x}} \Theta_{\ell}(k, t) \Theta_{\ell'}(k', t) Y_{\ell m}^*(\hat{\mathbf{k}}) Y_{\ell' m'}^*(\hat{\mathbf{k}}') (2\pi)^3 \delta^{(3)}(\mathbf{k} + \mathbf{k}') \frac{2\pi^2}{k^3} \sum_{LM} g_{LM}(k) Y_{LM}(\hat{\mathbf{k}}). \quad (\text{A.10})$$

The 3-dimensional integral over \mathbf{k}' is trivial due to the δ function and the 3-dimensional integral over \mathbf{k} is split into a radial part and an angular part:

$$C(\hat{\mathbf{n}}, \hat{\mathbf{n}}') = \sqrt{4\pi} \sum_{LM} \sum_{\ell m} \sum_{\ell' m'} (4\pi)^2 (-i)^{\ell+\ell'} \frac{1}{(2\pi)^3} Y_{\ell m}(\hat{\mathbf{n}}) Y_{\ell' m'}(\hat{\mathbf{n}}') \int_0^{\infty} dk k^2 \frac{2\pi^2}{k^3} g_{LM}(k) \Theta_{\ell}(k, t) \Theta_{\ell'}(k, t) \int d\hat{\mathbf{k}} Y_{LM}(\hat{\mathbf{k}}) Y_{\ell m}^*(\hat{\mathbf{k}}) Y_{\ell' m'}^*(-\hat{\mathbf{k}}). \quad (\text{A.11})$$

Using $Y_{\ell' m'}(-\hat{\mathbf{k}}) = (-1)^{\ell'} Y_{\ell' m'}(\hat{\mathbf{k}}) = (-i)^{2\ell'} Y_{\ell' m'}(\hat{\mathbf{k}})$ we get

$$C(\mathbf{n}, \mathbf{n}') = \sqrt{4\pi} \sum_{LM} \sum_{\ell m} \sum_{\ell' m'} (4\pi)^2 (-i)^{\ell+\ell'} \frac{1}{(2\pi)^3} Y_{\ell m}(\hat{\mathbf{n}}) Y_{\ell' m'}(\hat{\mathbf{n}}') \int_0^{\infty} dk k^2 \frac{2\pi^2}{k^3} g_{LM}(k) \Theta_{\ell}(k, t) \Theta_{\ell'}(k, t) \int d\hat{\mathbf{k}} Y_{LM}(\hat{\mathbf{k}}) Y_{\ell m}^*(\hat{\mathbf{k}}) (-i)^{-2\ell'} Y_{\ell' m'}^*(\hat{\mathbf{k}}), \quad (\text{A.12})$$

where the numerical factors may be combined, and factors shuffled, to write:

$$C(\hat{\mathbf{n}}, \hat{\mathbf{n}}') = \sqrt{4\pi} \sum_{LM} \sum_{\ell m} \sum_{\ell' m'} (4\pi) (-i)^{\ell-\ell'} Y_{\ell m}(\hat{\mathbf{n}}) Y_{\ell' m'}(\hat{\mathbf{n}}') \int_0^{\infty} \frac{dk}{k} g_{LM}(k) \Theta_{\ell}(k, t) \Theta_{\ell'}(k, t) \int d\hat{\mathbf{k}} Y_{LM}(\hat{\mathbf{k}}) Y_{\ell m}^*(\hat{\mathbf{k}}) Y_{\ell' m'}^*(\hat{\mathbf{k}}). \quad (\text{A.13})$$

Now

$$\int d\hat{\mathbf{k}} Y_{LM}(\hat{\mathbf{k}}) Y_{\ell m}^*(\hat{\mathbf{k}}) Y_{\ell' m'}^*(\hat{\mathbf{k}}) = (-1)^{m'} \sqrt{\frac{(2\ell+1)(2\ell'+1)}{4\pi(2L+1)}} C_{\ell 0 \ell' 0}^{L 0} C_{\ell m \ell' -m'}^{LM}, \quad (\text{A.14})$$

and the factors of $\sqrt{4\pi}$ cancel, yielding

$$C(\hat{\mathbf{n}}, \hat{\mathbf{n}}') = \sum_{LM} \sum_{\ell\ell'} \sum_{mm'} Y_{\ell m}(\hat{\mathbf{n}}) Y_{\ell' m'}(\hat{\mathbf{n}}') C_{\ell m \ell' -m'}^{LM} (-1)^{m'} C_{\ell 0 \ell' 0}^{L0} \sqrt{\frac{(2\ell+1)(2\ell'+1)}{(2L+1)}} \\ \times \left[4\pi (-i)^{\ell-\ell'} \int_0^\infty d \log k g_{LM}(k) \Theta_\ell(k, t) \Theta_{\ell'}(k, t) \right]. \quad (\text{A.15})$$

The square brackets isolate the BipoSH coefficients from the (WMAP normalised) basis functions and the expression matches eq.(2.8) after identifying Θ with Δ .

B Other choices of λ

We present here the reconstructions for other values of the regularisation parameter λ . The results for $\lambda = 500$ are shown in Fig. 17. Note the feature at $k \sim 0.006 \text{ Mpc}^{-1}$ which persists when λ is increased to 1000 as shown in Fig. 18. The reconstructions for $\lambda = 10000$ are shown in Fig. 19. The quadrupole modulation g_{2M} at $k \sim 0.006 \text{ Mpc}^{-1}$ is tabulated in Table 5.

M	$10^9 \text{ Re } g_{2M}$	$10^9 \text{ Im } g_{2M}$
0	-0.21 ± 0.18	
1	0.20 ± 0.15	0.09 ± 0.15
2	-0.16 ± 0.14	0.56 ± 0.14

Table 5. The quadrupole modulation at $k \sim 0.006 \text{ Mpc}^{-1}$ with frequentist errors, from the reconstruction with $\lambda = 100$.

C The distribution of T

It is shown below that the test statistic in eq.(5.7):

$$T(g_{2M}, \lambda) = (\mathbf{g}^{2M})^T \Sigma_{\text{F}}^+ (\mathbf{g}^{2M}), \quad (\text{C.1})$$

follows a χ^2 distribution with degrees of freedom equal to the rank of the pseudoinverse of the covariance matrix.

Let the $N \times N$ covariance matrix Σ_{F} be diagonalised as

$$\Sigma_{\text{F}} = \mathbf{U} \mathbf{D} \mathbf{U}^T, \quad (\text{C.2})$$

where \mathbf{D} is a diagonal matrix. The pseudoinverse of the covariance matrix then reads

$$\Sigma_{\text{F}}^+ = \mathbf{U} \tilde{\mathbf{D}} \mathbf{U}^T \quad (\text{C.3})$$

where $\tilde{\mathbf{D}}$ is the matrix that results from replacing the non-zero diagonal elements by their reciprocal. Further decompose $\tilde{\mathbf{D}}$ into $\tilde{\mathbf{D}} = \tilde{\mathbf{D}}^{1/2} (\tilde{\mathbf{D}}^{1/2})^T$ such that

$$\Sigma_{\text{F}}^+ = \mathbf{U} \tilde{\mathbf{D}}^{1/2} (\tilde{\mathbf{D}}^{1/2})^T \mathbf{U}^T, \quad (\text{C.4})$$

where $\tilde{\mathbf{D}}^{1/2}$ is a matrix with the diagonal elements equal to the square root of those of \mathbf{D} and with the zero columns removed. There are $N - \text{rank}(\Sigma_{\text{F}}^+)$ such columns. Transform to new variables

$$\mathbf{y}^{2M} = (\tilde{\mathbf{D}}^{1/2})^T \mathbf{U}^T \mathbf{g}^{2M}, \quad (\text{C.5})$$

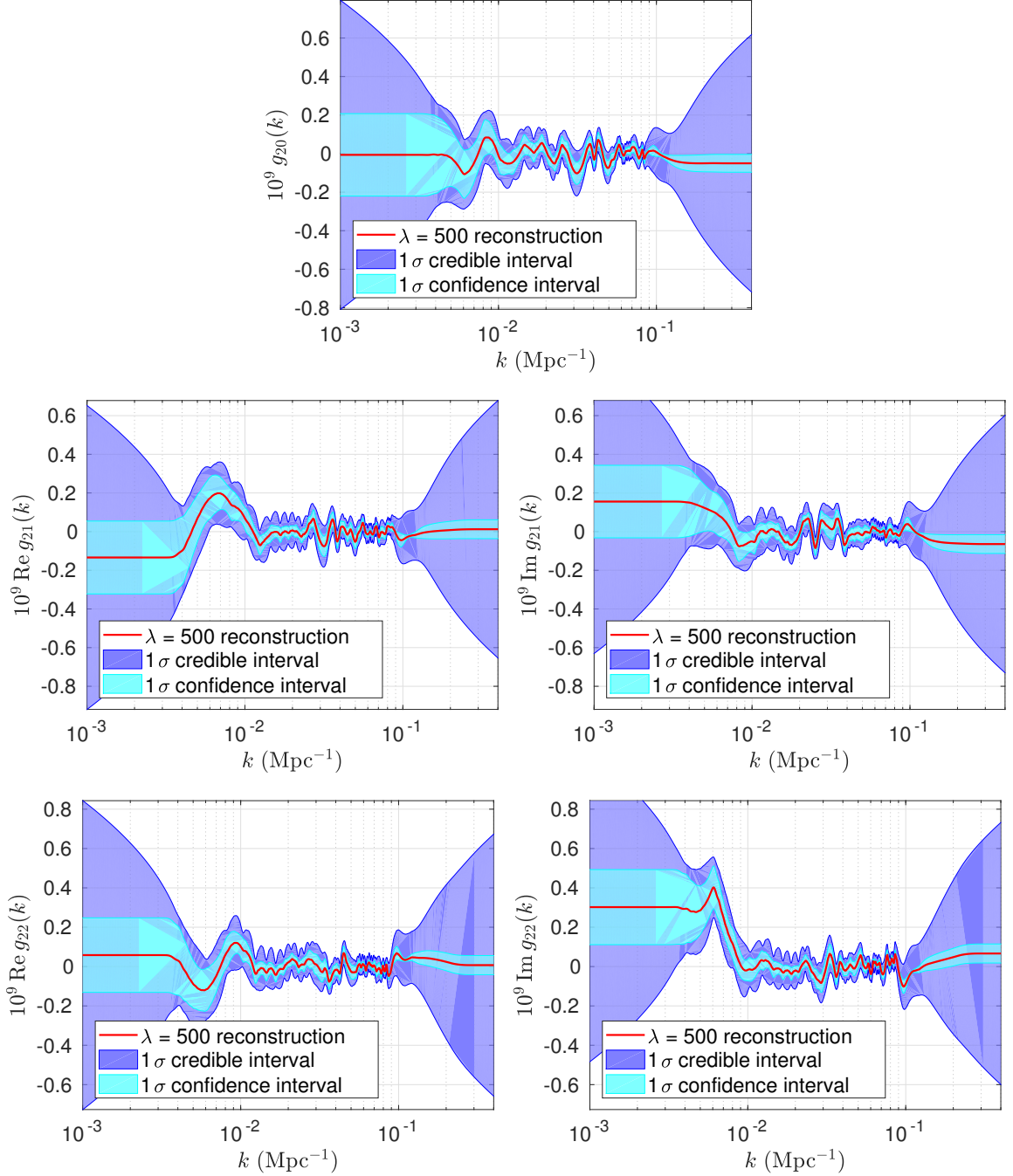


Figure 17. Reconstructed quadrupole modulation (full red line) with 1σ credible intervals (purple) and 1σ confidence intervals (cyan) for $\lambda = 500$. Note the feature in $\text{Im } g_{21}$ at $k \sim 0.006 \text{ Mpc}^{-1}$.

which is a variable of dimension $\text{rank}(\Sigma_{\text{F}}^+)$ and the test statistic becomes

$$T(y_{2M}, \lambda) = (\mathbf{y}^{2M})^T \mathbf{y}^{2M}. \quad (\text{C.6})$$

If each component of \mathbf{y}^{2M} is distributed according to a univariate Gaussian distribution, then T , which consists of a sum of squares of such variables, has a χ^2 distribution with degrees of

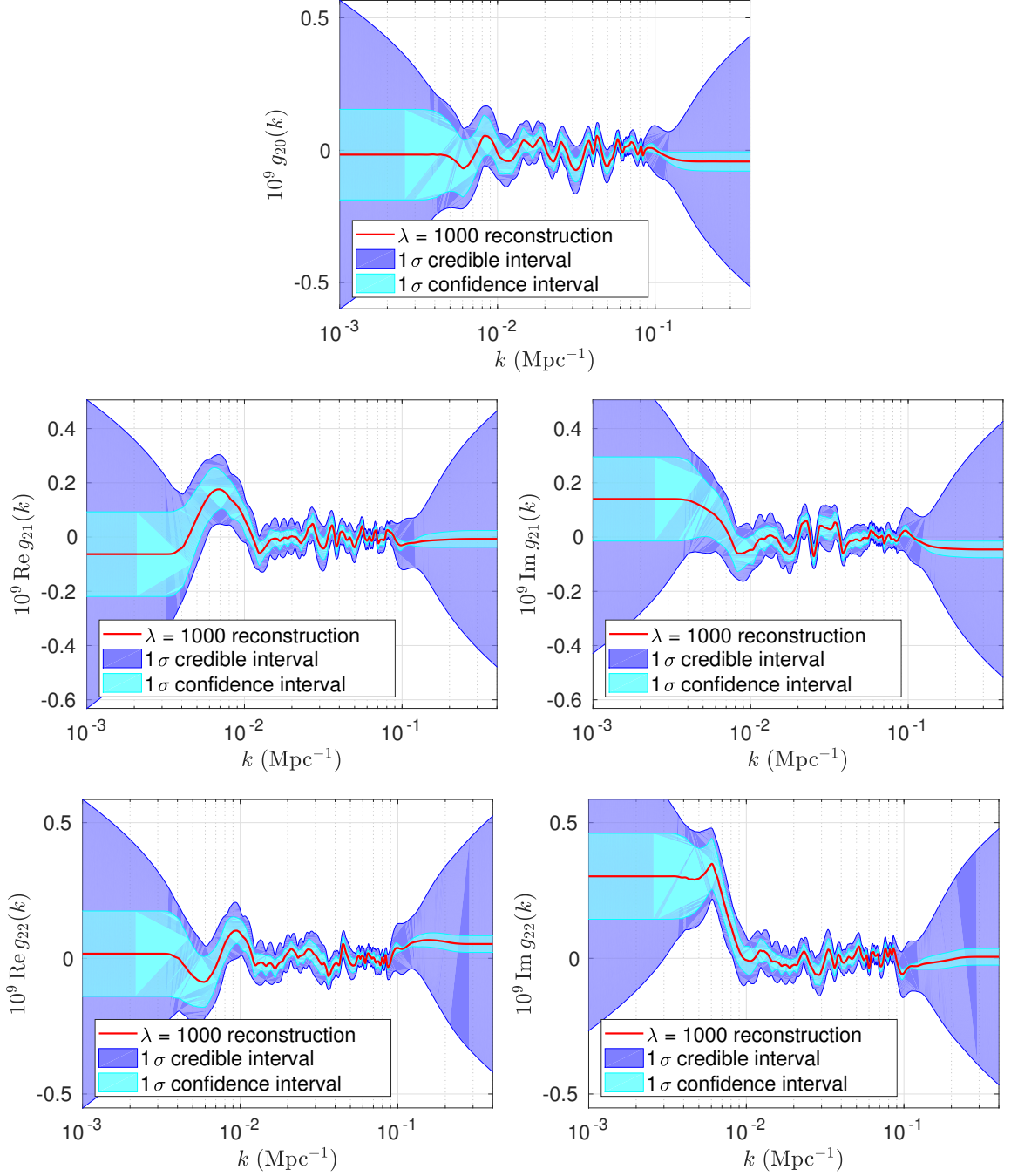


Figure 18. Reconstruction for $\lambda = 1000$.

freedom equal to the number of variables, namely $\text{rank}(\Sigma_F^+)$. This is indeed the case, as the covariance matrix equals the identity matrix

$$\langle \mathbf{y}^{2M} (\mathbf{y}^{2M})^T \rangle = \langle (\tilde{\mathbf{D}}^{1/2})^T \mathbf{U}^T \mathbf{g}^{2M} (\mathbf{g}^{2M})^T \mathbf{U} \tilde{\mathbf{D}}^{1/2} \rangle, \quad (\text{C.7})$$

and the expectation values may be taken to exclude the constant parts so that

$$\langle \mathbf{y}^{2M} (\mathbf{y}^{2M})^T \rangle = (\tilde{\mathbf{D}}^{1/2})^T \mathbf{U}^T \langle \mathbf{g}^{2M} (\mathbf{g}^{2M})^T \rangle \mathbf{U} \tilde{\mathbf{D}}^{1/2}, \quad (\text{C.8})$$

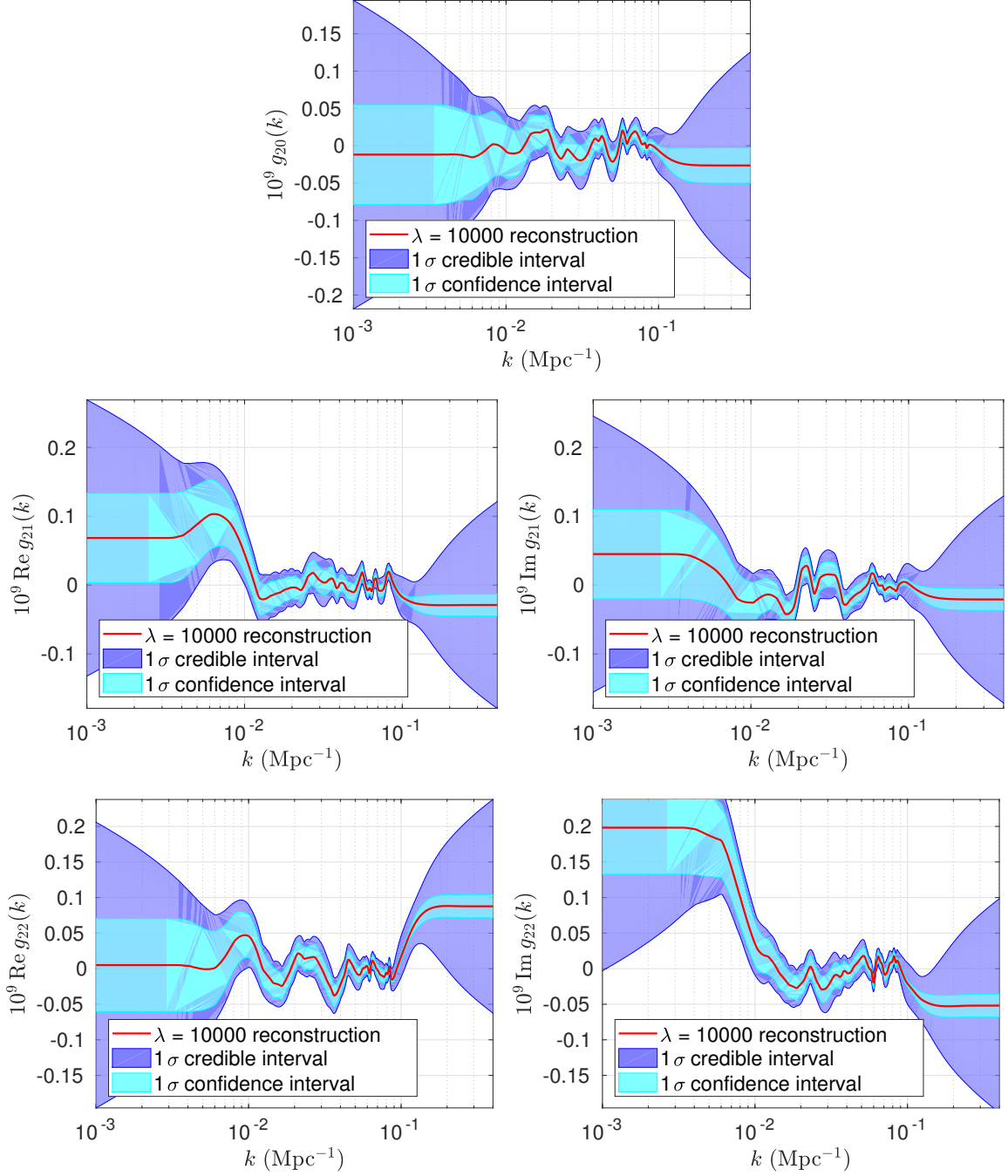


Figure 19. Reconstruction for $\lambda = 10000$.

and evaluated to give the frequentist covariance matrix Σ_F :

$$\langle \mathbf{y}^{2M} (\mathbf{y}^{2M})^T \rangle = (\tilde{\mathbf{D}}^{1/2})^T \mathbf{U}^T \Sigma_F \mathbf{U} \tilde{\mathbf{D}}^{1/2}. \quad (\text{C.9})$$

Expressing this in the diagonalised form (C.2) and reordering we get

$$\langle \mathbf{y}^{2M} (\mathbf{y}^{2M})^T \rangle = (\tilde{\mathbf{D}}^{1/2})^T \mathbf{U}^T (\mathbf{U} \mathbf{D} \mathbf{U}^T) \mathbf{U} \tilde{\mathbf{D}}^{1/2} \quad (\text{C.10})$$

$$= (\tilde{\mathbf{D}}^{1/2})^T (\mathbf{U}^T \mathbf{U}) \mathbf{D} (\mathbf{U}^T \mathbf{U}) \tilde{\mathbf{D}}^{1/2} = (\tilde{\mathbf{D}}^{1/2})^T \mathbf{D} \tilde{\mathbf{D}}^{1/2} = \mathbf{I}, \quad (\text{C.11})$$

since $\mathbf{U}^T \mathbf{U} = \mathbf{I}$ (\mathbf{U} is orthogonal as $\Sigma_{\mathbf{F}}$, the matrix being diagonalised, is symmetric).

D The Anderson-Darling test

The Anderson-Darling test [22] checks if a particular sample is likely to have come from a given distribution. Consider a sample x_1, x_2, \dots, x_n of a stochastic variable X . When this is sorted in ascending order $x_{(1)}, x_{(2)}, \dots, x_{(n)}$, the empirical distribution function $F_n(x)$ can be constructed as the fraction of the sample that has values less than or equal to x . In asking if a sample is likely to come from a probability distribution $P(x, \boldsymbol{\theta})$, where $\boldsymbol{\theta}$ denotes the set of parameters specifying the probability distributions, the empirical distribution function $F_n(x)$ may be compared with the cumulative distribution function $F(x, \boldsymbol{\theta}) = \int_{-\infty}^x dy P(y, \boldsymbol{\theta})$ as a weighted square error in the test statistic

$$W^* = n \int_{-\infty}^{\infty} dF(x) (F_n(x) - F(x, \boldsymbol{\theta}))^2 \psi(x), \quad (\text{D.1})$$

where, for the Anderson-Darling test, $\psi(x) = (F(x, \boldsymbol{\theta})(1 - F(x, \boldsymbol{\theta})))^{-1}$. For the Gaussian distribution $\boldsymbol{\theta} = (\mu, \sigma)$ and $F(x, \boldsymbol{\theta}) = (2\pi\sigma^2)^{-1/2} \int_{-\infty}^x \exp(-(x - \mu)^2/(2\sigma^2))$.

In practice, another form is used. Upon calculating $z_{(i)} = F(x_{(i)}, \boldsymbol{\theta})$, the Anderson-Darling statistic is

$$A_n^2 = -n^{-1} \sum_{x=1}^n (2i - 1)(\log z_i + \log(1 - z_{n+1-i})) - n. \quad (\text{D.2})$$

Rejection at a given significance level is then based on the value of A_n^2 being greater than a tabulated value. If the parameters of the distribution $\boldsymbol{\theta}$ are unknown they are replaced by the average and the sample standard deviation of the sample. It is then necessary to modify the test statistic in order to take this additional uncertainty into account so that $A^* = A_n^2(1 + b_0/n + b_1/n^2)$ and then compare with tabulated values [25].

Alternatively, the significance level may be assessed by generating a large number of samples taken from a Gaussian distribution with zero mean and unit variance. For each, the *sample* standard deviation is used as standard deviation and the *mean* as average. Then the test statistic (D.2) is computed. The test statistic obtained for the original is then compared with the distribution of test statistics for the simulated samples to assess the significance.

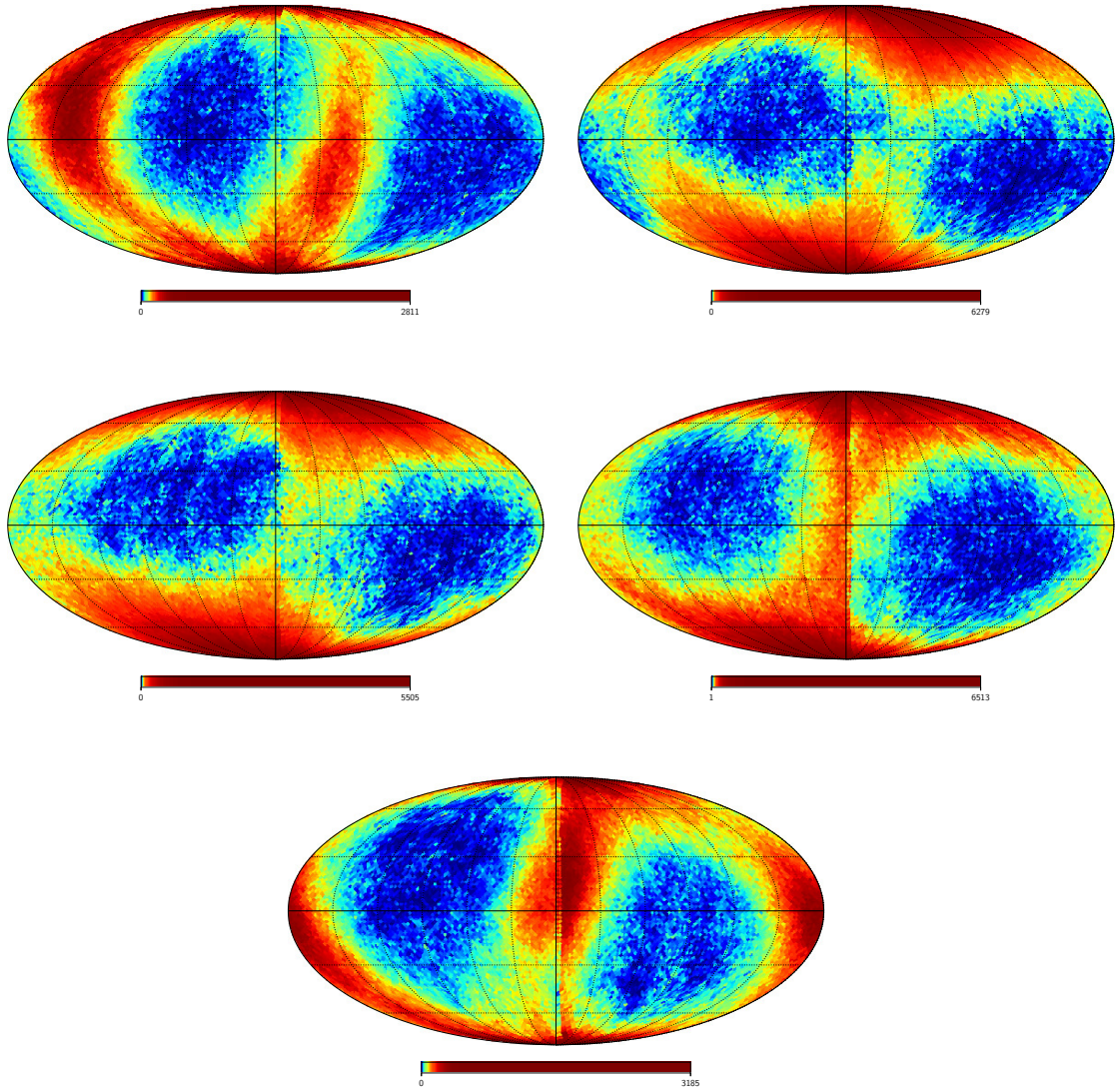


Figure 20. Equalised histograms of possible *directions* of the quadrupole modulation for power law modulations of the form $g_{2M}(k) \propto (k/k_*)^q$ ranging from $q = -2$ (upper left figure) to $q = 2$ (centred lower figure) derived from Monte Carlo runs.

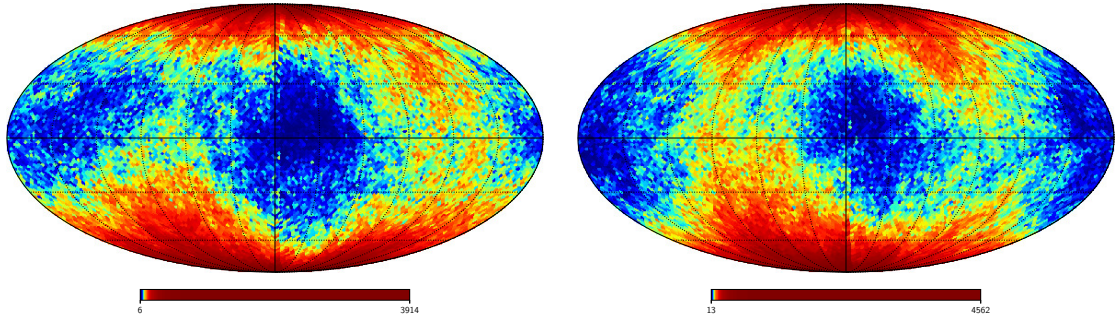


Figure 21. Mollweide projection of equalised histograms of possible *directions* $\hat{\mathbf{n}}_1$ (left image) and $\hat{\mathbf{n}}_2$ (right image) of the (most general) *scale-independent* quadrupole modulation derived from Monte Carlo runs.

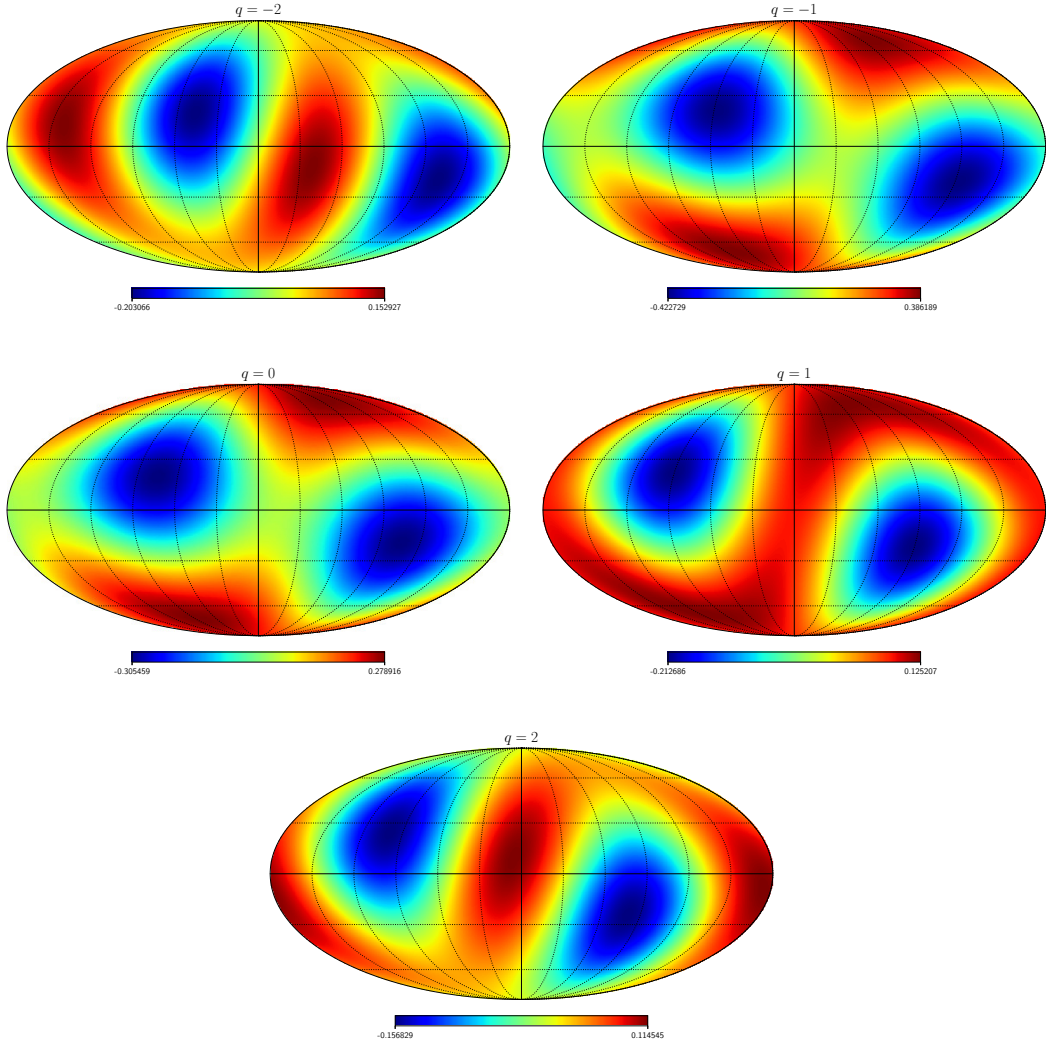


Figure 22. Mollweide projection of the best-fit power law quadrupole modulation $g_{2M}(k) \propto \mathcal{P}(k)(k/k_*)^q$ ranging from $q = -2$ to $q = 2$.

M	$10^2 \times \text{Re } g_{2M\star}$	$10^2 \times \text{Im } g_{2M\star}$	M	$10^2 \times \text{Re } g_{2M\star}$	$10^2 \times \text{Im } g_{2M\star}$
$q = -2$			$q = 2$		
0	0.04 ± 0.14		0	0.02 ± 0.12	
1	0.09 ± 0.11	-0.06 ± 0.10	1	-0.03 ± 0.07	-0.09 ± 0.07
2	0.03 ± 0.11	0.21 ± 0.11	2	0.15 ± 0.07	-0.05 ± 0.07
$q = -1$			$q = 1$		
0	0.44 ± 0.40		0	0.12 ± 0.21	
1	0.14 ± 0.27	-0.32 ± 0.27	1	-0.01 ± 0.13	-0.15 ± 0.13
2	0.07 ± 0.27	0.23 ± 0.27	2	0.17 ± 0.13	0.00 ± 0.13

Table 6. Power-law quadrupole modulations of the form $g_{2M} \propto g_{2M\star}(k/k_*)^q \mathcal{P}(k)$.